

# Open Research Online

---

The Open University's repository of research publications and other research outputs

## The source of A-type magmas in two contrasting settings: U–Pb, Lu–Hf and Re–Os isotopic constraints

### Journal Item

How to cite:

Pankhurst, M. J.; Schaefer, B. F.; Turner, S. P.; Argles, T. and Wade, C. E. (2013). The source of A-type magmas in two contrasting settings: U–Pb, Lu–Hf and Re–Os isotopic constraints. *Chemical Geology*, 351 pp. 175–194.

For guidance on citations see [FAQs](#).

© 2013 Elsevier B.V.

Version: Accepted Manuscript

Link(s) to article on publisher's website:

<http://dx.doi.org/doi:10.1016/j.chemgeo.2013.05.010>

---

Copyright and Moral Rights for the articles on this site are retained by the individual authors and/or other copyright owners. For more information on Open Research Online's data [policy](#) on reuse of materials please consult the policies page.

---

[oro.open.ac.uk](http://oro.open.ac.uk)

1  
2  
3  
4  
5  
6  
7  
8  
9  
10  
11  
12  
13  
14  
15  
16  
17  
18  
19  
20  
21  
22  
23  
24  
25  
26  
27  
28  
29  
30

The source of A-type magmas in two contrasting settings: U–Pb, Lu–Hf and Re–Os isotopic constraints.

<sup>1</sup>Pankhurst, M. J., <sup>1</sup>Schaefer, B. F., <sup>1</sup>Turner, S. P., Argles, T.<sup>2</sup>, Wade, C. E.<sup>3</sup>

<sup>1</sup>GEMOC, Macquarie University, Sydney 2109, Australia

<sup>2</sup>Department of Earth and Environmental Sciences,  
The Open University, Milton Keynes, MK7 6AA, UK

<sup>3</sup>Geological Survey of South Australia, Department for Manufacturing, Innovation, Trade, Resources  
and Energy (DMITRE), GPO Box 1264 Adelaide, South Australia, 5001

Corresponding author: Matthew J. Pankhurst [matt.pankhurst@gmail.com](mailto:matt.pankhurst@gmail.com)

Keywords: Re–Os isotopes, A-type, U–Pb isotopes, Lu–Hf isotopes, post-orogenic, geodynamics, lithospheric stabilization.

31

32

33 **Abstract:** The source of post orogenic A-type magmas from two distinct geodynamic  
34 settings are compared. The end of the ca. 514 – 480 Ma Delamerian Orogeny,  
35 southeastern South Australia, was marked by ~10 Myr of bimodal A-type  
36 magmatism, driven by convective removal of thickened lithosphere. Initial Os and Hf  
37 isotope ratios record a heterogeneous lithospheric mantle source, with some input  
38 from aesthenospheric mantle. Mafic parental melts fractionated to produce the  
39 granites. In contrast, initial Os isotope ratios of the A-type magmas that comprise the  
40 ca. 1598 – 1583 Ma Mesoproterozoic Gawler Felsic Large Igneous Province, central  
41 South Australia, record a dominant evolved lower crust component. However, initial  
42 Hf isotope ratios from these samples are depleted, indicating a mantle source for  
43 lithophile elements. This voluminous, bimodal magmatism lasted for ~15 Myr, and  
44 ended the Wartakan Orogeny. In both cases the homogenisation of chemical  
45 (rheological) heterogeneities, inherited from terrain amalgamation and orogenic  
46 thickening, strengthened the lithosphere. The contemporaneous fusion of  
47 heterogeneous mantle ± crust may represent a common, stabilizing influence on the  
48 lithospheric column regardless of tectono-magmatic setting.

49

50 **Introduction:**

51

52 A-type magmas form a distinctive subset of igneous rocks. As a group, A-type  
53 granitoids are recognized as possessing a large number of mineralogical and  
54 geochemical affinities, that serve to clearly distinguish them from I- and S-type  
55 granitoids in the majority of cases (e.g. Collins et al., 1982). Importantly, their initial  
56 radiogenic isotope ratios are most often juvenile (e.g. Kemp et al., 2009; Turner et al.,  
57 1992), their temperatures high (e.g. King et al., 2001; Turner et al., 1992) and their  
58 emplacement depths shallow (Bonin, 2007). These features suggest a deep rooted  
59 mantle source region and influence of the magmatic system across the entire  
60 lithospheric column.

61 A-types granitoids (hereafter termed A-types) occur in a number of tectonic  
62 settings. First named as such by Loiselle and Wones (1979) due to their ‘anorogenic,  
63 anhydrous and alkalic’ nature, A-types have subsequently been variably attributed to  
64 particular tectonic settings and melt source regions. Initially recognized as granites  
65 that occur along continental rift zones (Loiselle and Wones, 1979), A-types are also  
66 observed in post-collisional settings (Dargahi et al., 2010; Menuge et al., 2002) and as  
67 felsic portions of mafic large igneous provinces (e.g. Pankhurst et al., 2011a; Turner  
68 and Rushmer, 2009). Since A-types do not have one prevalent tectono-magmatic  
69 association (c.f. tholeiitic; mantle decompression melting, calc-alkaline; subduction  
70 zones), it is inappropriate to ascribe the mere presence of A-types to a single  
71 geodynamic setting.

72 An alternate approach is to use this apparently non-unique-setting magma type to  
73 highlight a potentially common influence upon the lithosphere, regardless of tectonic  
74 setting. Intriguingly, many A-type magmatic systems occur during the final stages of  
75 whichever tectono-magmatic expression they are a part of, and usually precede long  
76 periods of relative inactivity (e.g. Goodge and Vervoort, 2006; Puura and Flodén,  
77 1999; Rämö and Haapala, 1995). Are A-types a cause, or effect, of a strengthened  
78 lithosphere? If a common influence is discovered, A-type magmas may have greater  
79 utility in geodynamic models.

80 It is widely accepted that rheological heterogeneity plays a fundamental role in  
81 determining the bulk strength of a lithospheric domain (e.g. Kelemen and Hirth, 2007;  
82 Paczkowski et al., 2012; Platt and Behr, 2011; Vissers et al., 1995). Often ‘runaway’  
83 deformation is observed (or modeled), which is focused within shear zones that

84 accommodate strain by grain size reduction and/or involvement of a liquid (melt)  
85 phase (e.g. Kelemen and Dick, 1995; Paczkowski et al., 2012; Sundberg et al., 2010).  
86 Chemical (and isotopic) heterogeneity is a product of such processes (e.g. Homburg et  
87 al., 2010), as well as metasomatic processes. Thus all else being equal, a chemically  
88 heterogeneous lithospheric domain is weaker than a chemically homogeneous domain  
89 (e.g. Vissers et al., 1995). Removing heterogeneity from a lithospheric domain is, by  
90 extension, a mechanism for lithospheric strengthening. In this contribution we explore  
91 the potential role that high temperature magmatism plays in homogenizing a  
92 lithospheric domain by causing widespread fusion of damaged, heterogeneous  
93 material and promoting pathways for mixing between distinct sources  
94 (homogenization). This post-orogenic re-organisation of high chemical (physical)  
95 gradients into low chemical gradients may serve to promote a stronger local  
96 lithosphere.

97 Should such magmatism play role in, or simply be a record of, lithospheric  
98 strengthening (and hence –cratonisation), it is important to establish the ultimate  
99 source(s) and drivers of A-type provinces. These constraints can then be used to  
100 interrogate the geologic record in order to elucidate timing and duration of the onset  
101 of lithospheric stabilization. We explore the role of source in the petrogenesis of two  
102 adjacent, yet tectonically and temporally distinct A-type magmatic provinces from an  
103 isotopic perspective. Through a unique combination of Os and Hf isotopic techniques  
104 we evaluate the relative contributions of crust and mantle in the resultant granitoids  
105 and are able to highlight for the first time how a convergence of processes in the  
106 petrogenesis of these magmas can obscure some of the conventional isotopic signals  
107 relied upon in understanding the origin of these systems. We then comment on the  
108 implications of such magmatism in the formation of stable lithospheric columns and  
109 the preservation of continents.

110

111 Characteristics and petrogenesis of A-types

112

113 A-types most often display anhydrous mineralogy which is characterized by alkali  
114 feldspar + quartz > plagioclase > ferromagnesian + oxide minerals > accessory  
115 minerals (apatite, fluorite, zircon, titanite, other phosphates). A-types may display  
116 hypersolvus, transsolvus or subsolvus alkali feldspar (Bonin, 2007). Geochemical  
117 affinities include comparatively high Fe/Mg, (K+Na)/Al, Ga/Al and K/Na, elevated

118 rare earth and high field strength element (REE & HFSE) and F content, and light rare  
119 earth element (LREE) enrichment, resulting in ‘gull-wing’ normalized REE patterns  
120 (e.g. Creaser et al., 1991; Whalen et al., 1987). They range from peraluminous to  
121 peralkaline to metaluminous, sometimes within a single province (e.g. Shellnutt and  
122 Zhou, 2007). Low O<sub>2</sub> fugacity and high temperatures up to ~1100 °C (Frost and Frost,  
123 1997; Whalen et al., 1987) are also common and important features.

124 Eby (1992) suggested that two groups of A-types are observed. A1 are those with  
125 element ratios similar to ocean island basalts (OIB), and form via crystal fractionation  
126 from melts of the same sources. A2 are those that display geochemical affinities with  
127 post-collisional continental or island arc crust, and have been suggested to form by  
128 partial melting of a previously I-type-granite-depleted lower crust (e.g. Clemens et al.,  
129 1986). However, Creaser et al. (1991) suggest this residual-source model is unlikely  
130 to account for all the mineralogical and geochemical observations. These authors  
131 demonstrated that A-types could be generated by partial melting of an undepleted,  
132 water poor crustal source with tonalitic-granodioritic composition. For a recent review  
133 of A-type petrogenesis, see Dall’Agnol et al. (2012).

134 Such geochemical variations within the group of granitoids termed ‘A-type’ imply  
135 significantly different genesis in terms of their source, the degree of melting involved,  
136 and therefore thermal gradient. However, the most important factors in terms of  
137 physical properties of A-type felsic liquids; high temperature, alkali-rich major  
138 element chemistry, concentration of water (low) and halogens (high), are key  
139 characteristics of the group. Further, the corollary is that the material left behind  
140 during A-type extraction by either partial melting or fractionation will also bear a  
141 chemical resemblance to each other (Turner and Rushmer, 2009), which implies  
142 similar physical properties.

143 Importantly, the volume of material that is either cumulate or residue is also  
144 predicted to be relatively similar. For instance, Turner et al. (1992) modeled some A-  
145 types as the product of ~90% crystallization of a contemporary tholeiitic magma. The  
146 residual volume after extraction of an A-type liquid by partial melting is identical if  
147 the source is basaltic (Turner and Rushmer, 2009). Rocchi et al. (2009) estimated that  
148 ~20% partial melting of intrusive lamprophyres at the base of the crust could produce  
149 the observed A-types (albeit not strictly anhydrous in this example). In both instances  
150 the formation of a depleted mafic body at depth is implied. The key difference is that  
151 A-types formed by extreme (closed system) fractionation require a coeval volume of

152 mafic magma ~10x that of the granite volume. A-types formed by partial melting do  
153 not require large mafic magma chambers, as their source region could plausibly  
154 accumulate by iterative addition of small volume mafic melts.

155

156 Determining the source of A-type magmas

157

158 Radiogenic isotope ratios from A-types are most often juvenile (e.g. Kemp et al.,  
159 2009; Turner and Foden, 1996; Turner et al., 1992) —although not in every case (e.g.  
160 Huang et al., 2011)— and thus A-type magmas have been attributed with forming  
161 new granitic continental crust (c.f. recycling/maturation of older continental crust via  
162 I- and S- type magmatism; Villaseca et al., 2012). However, in many cases juvenile  
163 isotope ratios can also explained by the partial melting of juvenile crust and enriched  
164 mantle, and variable hybridization between these coeval magmas (e.g. Rutanen et al.,  
165 2010).

166 Traditional debate of A-types surrounds the role of mantle contributions to the  
167 crust over time, historically assessed by Nd-, and more recently Hf-isotope systems  
168 (e.g. Kemp et al., 2009). Both these systems reflect lithophile behaviour, but  
169 potentially may misrepresent a suspected mantle component, due to inheritance via  
170 magma assimilation or mingling (e.g. Pankhurst et al., 2011c). The Lu-Hf system  
171 broadly approximates the Sm-Nd, however due to the relative difference in D values,  
172 the Lu-Hf system is less affected by AFC processes (following the models of  
173 DePaolo, 1981). A distinct advantage for our purposes is that Hf in A-types (as in  
174 other granitoids) is primarily located within zircons. Thus inheritance of Hf can be  
175 clearly delineated through combined analysis with U-Pb geochronology. Zircons in  
176 granitoids contain Hf in concentrations of up to a few wt%, and contain comparatively  
177 little Lu (median = 150 ppm; Belousova et al., 2002) that would otherwise represent a  
178 source of uncertainty. Thus the initial Hf isotope ratio of the equilibrium liquid is  
179 preserved within magmatic zircon. Importantly, ingrowth of radiogenic Hf can be  
180 accurately age-corrected by U–Pb isotope analysis of the same region of zircon  
181 (Belousova et al., 2009).

182 A novel approach to the problem of A-type source regions is to utilise the Re-Os  
183 system. The  $^{187}\text{Re}$ - $^{187}\text{Os}$  decay scheme is most commonly used to inform siderophile  
184 and chalcophile element, and hence mantle, behaviour (e.g. Schaefer et al., 2010).  
185 However, very high Re/Os ratios in continental crust also make this system a very

186 sensitive monitor of crustal contributions to mantle derived magmas (e.g. Gregory et  
187 al., 2008; Shirey and Walker, 1998). For example, average continental crust is ~20  
188 times more radiogenic than chondrite, and ancient lithospheric mantle contains sub-  
189 chondritic Os isotope ratios (Schaefer et al., 2000). A combined approach, using both  
190 Lu-Hf and Re-Os as a tool for mantle and crustal contributions to magmas, is  
191 underutilized despite this value (see Johnson et al., 1996).

192

### 193 **Geologic Setting:**

194

195 Undeformed plutons and associated volcanics of the Padthaway Ridge, southeastern  
196 South Australia, occur as an arcuate chain of A-type bodies that extends for ~300 km  
197 (Fig. 1a). These magmas represent the final tectono-thermal expression of the  
198 Delamerian Orogeny (~514-490 Ma; Foden et al., 2006), the first of a series of  
199 eastward-younging orogenies accreted to then Gondwanan margin, driven by a supra-  
200 subduction system (e.g. Kemp et al. 2009) The A-types are hypothesised to have  
201 formed when convective removal of overthickened lithospheric mantle led to rapid  
202 exhumation of the fold belt (Turner et al., 1996b). Post-convergent extension is  
203 argued to have allowed mafic melts to ascend to shallow depths, where closed-system  
204 crystal fractionation, involving olivine, pyroxenes, plagioclase and Fe-oxides took  
205 place (Turner et al., 1992), without significant crustal assimilation (Foden et al.,  
206 2002b). The predicted large volumes of intrusive mafic equivalents and cumulates are  
207 consistent with the presence of a gravity and aeromagnetic anomaly coincident with  
208 the Padthaway Ridge (e.g. Kennedy, 1989).

209 Immediately west of the rocks of the Delamerian Orogeny is the Tasman Line, a  
210 largely inferred lithospheric scale structure dividing western Precambrian Australia  
211 from the younger eastern basement successions (e.g. Arroucau et al., 2010). The  
212 closest occurrence of post-orogenic A-type magmatism in Proterozoic terranes west of  
213 the Tasman Line is that of the Hiltaba Event (1600-1560 Ma; Betts et al., 2002),  
214 which represents the last tectono-thermal episode of the central Gawler Craton (Fig.  
215 1b) (Betts and Giles, 2006).

216 The Hiltaba Event is characterized by rapid, high temperature, voluminous and  
217 widespread bimodal A-type magmatism into and across a basement of  
218 Palaeoproterozoic and Archean rocks (Blissett et al., 1993; Pankhurst et al., 2011b).  
219 The voluminous Gawler Range Volcanics (GRV) were emplaced within 2 Myr at



220 1592 ± 2 Ma (Creaser, 1995; Fanning et al., 1988), extend for >25,000 km<sup>2</sup> (Blissett  
221 et al., 1993) and are overwhelmingly felsic (Allen et al., 2003). Basalts and basaltic  
222 andesites outcrop in just a few localities (Allen et al., 2008). Hiltaba Suite granitoids  
223 are considered the shallow intrusive equivalent to the GRV, crop out across much of  
224 the Gawler Craton, and span a longer time interval of emplacement, 1598 ±2 to 1583  
225 ± 7 (Flint, 1993). These granites display a provinciality in terms of Nd isotopes  
226 (Creaser, 1995), which are suggestive of appreciable crustal involvement, supported  
227 by the observation of inherited zircon cores (e.g. Creaser and Fanning, 1993 and  
228 references therein).

229 Together the GRV and Hiltaba Suite Granitoids comprise the Gawler Felsic Large  
230 Igneous Province (FLIP). A large, elliptical, gravity high is coincident with the main  
231 GRV province (see data in Rajagopalan et al., 1993), which is consistent with  
232 significant volumes of mafic material predicted to exist at depth (Stewart, 1994). This  
233 anomaly was modeled by Phillips (2006) who filtered shallow sources and concluded  
234 the source of the gravity high was present at mid crustal levels.

235 The Gawler FLIP was preceded by ~10-20 Ma of crustal shortening, termed the  
236 Wartarkan Orogeny, that took place immediately after arc magmatism on the southern  
237 Gawler Craton margin ceased (Stewart and Betts, 2010b). The geometry of this arc-  
238 related calc-alkaline magmatism, and that of the Musgrave arc to the north, places the  
239 Gawler FLIP within a post-back-arc environment (Swain et al., 2008; Wade et al.,  
240 2006). Betts et al. (2009; 2007) used a synthesis of geologic, geochronological and  
241 geophysical data to propose a model that describes a plume head arrival as triggering  
242 the voluminous A-type magmatism, and progressed as hotspot-like magmatism across  
243 the eastern terranes of Proterozoic Australia. This plume-head-modified subduction  
244 was modeled by Betts et al. (2012), who found that the switching-off of subduction  
245 magmatism, and compression in the overriding plate, was likely due to trench  
246 advance, and not flat subduction. In their model, the buoyant plume head opened a  
247 window in the subducting slab, and was therefore able to interact with the overriding  
248 plate, without major reorganization of the subduction zone.

249

250

## 251 **Samples and analytical techniques:**

252 Samples

253 The Delamerian A-type system is represented in this dataset by two granites,  
254 (Marcollat and Seismograph), a rhyolite (Mt. Monster Porphyry), and a coeval  
255 peridotite cumulate (Black Hill peridotite), encompassing ~300 km of orogenic strike  
256 length, see figure 1a. Details of these samples can be found in Turner et al. (1992) and  
257 Turner, (1996). We also analysed a representative sample of the ca. 525 Ma Truro  
258 Volcanics, which are small volume strongly undersaturated alkali basalts that erupted  
259 immediately prior to the Delamerian Orogeny (see Forbes et al., 1972; Turner and  
260 Foden, 1990), for Re-Os. This allows a comparison to be made on the nature of the  
261 lithospheric mantle, in terms of Re-Os, before and after the orogeny.

262 The Gawler FLIP is represented by the most mafic portions of the GRV accessible.  
263 They are from across the central Gawler Craton, and provide a ~350 km wide  
264 footprint, to assess source homogeneity, see figure 1b. Samples are from Chitalinga  
265 Hill (a basaltic trachyandesite), White Hill (troctolite), and Roopena Volcanics (basalt  
266 and trachybasalt). We also analysed samples of the A-type ca. 1560 Ma Sybella  
267 Granite, Mt. Isa Inlier, Queensland Australia for Re-Os. This is considered a northern  
268 extension of the Mesoproterozoic hotspot trail (Betts et al., 2007), and allows us to  
269 compare Re-Os sources across the Proterozoic terranes of Australia.

## 270 In-situ zircon analysis

271

272 Zircon fragments and complete crystals up to ~210  $\mu\text{m}$  from the Marcollat Granite  
273 (n=33) and Mount Monster Porphyry (n=35) were separated, hand picked, mounted in  
274 resin, and polished. The structure of the zircons were assessed by cathodoluminescence  
275 (CL) and back-scattered electron (BSE) imaging using a Cameca SX100 Electron  
276 Microprobe (EMP), which was also used to analyse ~1 $\mu\text{m}$  spots upon the grains for  
277 major elements, see figure 3.

278 A New Wave UP-213 laser ablation system (5 Hz repetition rate, 30  $\mu\text{m}$  spot size,  
279  $\lambda=213$  nm) with a small format cell was used to ablate the grains, and an attached  
280 Agilent 7200 Series ICPMS measured trace element, U, Th and Pb isotope  
281 concentrations. After  $\geq 60$  s background count time, ablation intervals were 60-120 s  
282 per grain depending on the depth of available crystal. Several spots per single grain  
283 were analysed in order to explore any variation of age or trace elements within single  
284 grains. Marcollat (n=33) and Mt. Monster zircons (n=35) were analysed in one  
285 session each. The total of 72 analyses of unknowns were bracketed into six runs by

286 the isotopically homogeneous GEMOC-GJ-1 zircon standard (n=16), used to correct  
287 for U/Pb fractionation. For details of the GEMOC-GJ-1 standard see Elhlour et al.  
288 (2006). Two well-characterised zircons; 91500 (n=8) and Mud Tank (n=4) were  
289 analysed as independent controls on reproducibility and accuracy of isotope ratios;  
290 each returned an average within  $2\sigma$  of the long-term  $^{207}\text{Pb}/^{206}\text{Pb}$  ratio mean reported  
291 by Belousova et al. (2009). The data was processed using GLITTER software  
292 (www.glitter-gemoc.com) to calculate isotope ratios. The analytical procedures for the  
293 U–Pb dating are described in detail in Jackson et al. (2004). Analyses of the NIST-  
294 610 glass trace element standard (n=8) bracketed the analyses at regular intervals. Hf  
295 concentrations, measured by EMP, were used as known values with which to equate  
296 ICPMS total counts with concentration.

297 Hf, Lu and Yb isotopes were measured by a New Wave UP-266 laser ablation  
298 system (5 Hz repetition rate, 40  $\mu\text{m}$  spot size) attached to a Nu-plasma multicollector  
299 ICP-MS. Typical ablation times were 100-120 s, and total Hf beams were between 1.5  
300 and 3 V, depending on the structure and size of the zircon and Hf content. Detailed  
301 analytical procedures including corrections for mass interference can be found in  
302 Belousova et al. (2009). A single session for each of the sample was bracketed by four  
303 analyses of the Mud Tank zircon standard ( $^{176}\text{Hf}/^{177}\text{Hf} = 0.282535 \pm 47$ , n = 12 and  
304  $0.282539 \pm 16$ , n=7 for the Marcollat Granite and Mount Monster respectively). In  
305 addition the Temora standard was used for Mount Monster ( $^{176}\text{Hf}/^{177}\text{Hf} = 0.282732$   
306  $\pm 39$  n=7) and 91500 for the Marcollat ( $^{176}\text{Hf}/^{177}\text{Hf} = 0.282352 \pm 9$ , n = 1), all errors  
307 reported are  $1\sigma$ . Care was taken to ablate spots immediately adjacent to U-Pb and  
308 trace element determinations, within the same CL imaged zone.

309

#### 310 Whole rock Hf isotope analysis

311 A whole rock digestion for Hf isotope analysis for the Seismograph Rocks sample  
312 used standard HF-HNO<sub>3</sub> and purification was performed by standard anion exchange  
313 column separation techniques at the Geochemical Analysis Unit (GAU) of GEMOC,  
314 Macquarie University. The method was the same as that used for Gawler FLIP  
315 samples (Fricke, 2005). Hf isotope ratios were analysed by multi-collector ICP-MS  
316 (Nu plasma) also at the GAU and corrected to interpolated Lu and Hf values from  
317 Turner et al. (1992). BHVO-2 was used as an internal standard and returned a

318  $^{176}\text{Hf}/^{177}\text{Hf}$  ratio of  $0.283089 \pm 18$  ( $2\sigma$ ). JMC475 was used as an external standard and  
319 returned a  $^{176}\text{Hf}/^{177}\text{Hf}$  ratio of  $0.282157 \pm 27$  ( $2\sigma$ ).

320

321 Whole rock Re–Os isotopic analysis

322

323 Re–Os methodology follows that of isotope dilution techniques described in Gregory  
324 et al. (2008). Whole-rock powders for each sample were spiked for Re and Os and  
325 digested in inverse aqua regia (8 ml 16N  $\text{HNO}_3$ , 4 ml 12N  $\text{HCl}$ ) by carius tube  
326 dissolution followed by solvent extraction using the methods of Shirey and Walker  
327 (1995) and Cohen and Waters (1996) as described in Lambert et al. (1998, 2000).  
328 Rhenium was purified following Os extraction using anion exchange chromatography  
329 (Lambert et al. 1998). Osmium was analysed by N-TIMS on either a Thermo-  
330 Finnigan Triton at Macquarie University, Australia or at the Open University, UK.  
331 The Os samples were loaded onto Pt filaments and analysed using a combination of  
332 peak hopping or static collection depending on beam intensity for a minimum of 100  
333 ratios and more typically 250.

334 Rhenium was determined using a Nu-Plasma multi-collector inductively coupled  
335 plasma mass spectrometer (MC-ICPMS) at the GAU or the Open University. A Re  
336 standard solution was analysed every five samples to monitor drift and fractionation.  
337 Mesoproterozoic samples were blank corrected using values of 1 pg Re and 1.4 pg Os  
338 with a  $^{187}\text{Os}/^{188}\text{Os}$  ratio of 0.165 (GAU; as per Gregory et al., 2008). Delamerian data  
339 were blank corrected using 0.23 pg Os with a  $^{187}\text{Os}/^{188}\text{Os}$  ratio of 0.2713 (Open  
340 University). This corresponds to corrections of up to 22% and 7%, respectively.  
341 Whole-rock standard (WPR-1) values averaged 10.8 ppb Re, 16.5 ppb Os with  
342  $^{187}\text{Os}/^{188}\text{Os}$  ratio of 0.14473, reproducing accepted values (e.g., Cohen and Waters  
343 1996).

344

## 345 **Results**

346

347 In-situ U–Pb and Lu–Hf data from the Marcollat and Mt. Monster samples are  
348 presented in Table 1a and 1b respectively. In-situ trace element data from the Mt  
349 Monster zircons is also presented in Table 1b. For Marcollat zircon images, trace

350 element results and discussion see Pankhurst (2012). Whole rock Re–Os and Lu–Hf  
351 data, and a summary of the in-situ Lu–Hf data are presented in Table 3.

352

353 In situ zircon results

354

355 Strong oscillatory CL zoning is ubiquitous in the Marcollat Granite zircons (Fig. 2a),  
356 as is almost total absence of macro-inclusions, see Pankhurst (2012). Where  
357 geochronological information was obtained on both a core and rim, U–Pb ages are  
358 within error of each other, and common Pb correction was not required (Table 1a).  
359 The age of the Marcollat Granite is determined to be  $480 \pm 2.5$  Ma  $n=28$  (Fig. 3a).

360 The Mount Monster Porphyry zircons typically have metamict and/or fractured  
361 cores and cleaner rims (Fig. 2b). The often complex fracturing resulted in U–Pb ages  
362 that are mostly discordant, probably due to a combination of both Pb-loss and  
363 presence of common Pb (Fig. 3b). The age of the Mt Monster Porphyry is determined  
364 to be  $485.2 \pm 6.9$  Ma  $n=11$ , the greater error reflecting the large number of discordant  
365 grains, which were discarded. One zircon core (rounded and non-metamict) from the  
366 Monster Porphyry returned a concordant age of  $3034 \pm 58$  Ma. The individual age of  
367 the rim of this grain is  $474 \pm 10.9$  Ma (concordant), which demonstrates that the  
368 presence of this Archean-aged zircon core is not a result of lab contamination.

369 The Mt. Monster zircons contain U, Th, Y, Hf and Yb abundances are typical of  
370 crustal granitoids (see Belousova et al., 2002). Rare earth elements vary by up to three  
371 orders of magnitude, La; 0.77–168 ppm, Ce; 3.8–1842 ppm, Pr; 0.37–58 ppm, Er; 3.3–  
372 2175 ppm, Tm; 3.4–496 ppm. The varying degree of fracturing and metamictisation  
373 most likely contributes to elevated REE (e.g. Belousova et al., 2006). Results of trace  
374 element abundances, including REE of the Marcollat zircons, are discussed in  
375 Pankhurst (2012). With the possible exception of Ti, trace elements do not correlate  
376 Hf isotope variation.

377 The Marcollat Granite zircon measured  $^{176}\text{Hf}/^{177}\text{Hf}$  ratios range from 0.282554 to  
378 0.282776, with an average of  $0.282603 \pm 0.000108$   $2\sigma$ . There is no correlation with  
379  $^{176}\text{Yb}/^{177}\text{Hf}$ , which ranges from 0.03385 to an outlier of 0.1849, indicating the small  
380 corrections applied due to Yb interference on mass 176 are appropriate. The Mt.  
381 Monster zircon measured  $^{176}\text{Hf}/^{177}\text{Hf}$  ratios range from 0.282525 to 0.282986, with an  
382 average of  $0.282652 \pm 0.000212$   $2\sigma$ . There is no correlation with  $^{176}\text{Yb}/^{177}\text{Hf}$ , which

383 ranges from 0.0393722 to an outlier at 0.252503, indicating these slightly larger  
384 corrections applied due to Yb interference are also appropriate.

385 The Marcollat zircons  $\epsilon\text{Hf}_i$ , calculated using a  $^{176}\text{Lu}$  decay constant of  $1.93 \times 10^{-11}$ ;  
386 Siguigna et al, (1982) from Blichert-Toft and Albarède (1997), range from +2.2 to  
387 +10.4, at 480 Ma. Mount Monster Porphyry zircon  $\epsilon\text{Hf}_i$  ranges from +0.1 to +17.5, at  
388 485 Ma. Both the Marcollat and Mt. Monster zircons are similarly aged, and contain a  
389 similar average and range of  $\epsilon\text{Hf}_i$  values.

390

391 Whole rock Lu-Hf results

392

393 The Seismograph Granite has a  $^{176}\text{Hf}/^{177}\text{Hf}$  ratio of 0.282701, and a  $^{176}\text{Lu}/^{177}\text{Hf}$  ratio  
394 of 0.002310 (calculated from Turner et al. 1992 using reasonable Yb/Lu and Zr/Hf  
395 ratios in A-types, see Table 3), resulting in an  $\epsilon\text{Hf}_i$  of 3.97. The Gawler FLIP samples  
396 measured  $^{176}\text{Hf}/^{177}\text{Hf}$  ratios range from 0.282168 at Chitanilga Hill, to 0.282397 at  
397 Roopena, and correspond to  $\epsilon\text{Hf}_i$  values of -1.73 and 4.95 respectively (Fricke, 2005).

398

399 Whole rock Re-Os results

400

401  $^{187}\text{Os}/^{188}\text{Os}_i$  for Delamerian samples ranges from 0.1051 to 0.1977. Compared with  
402 C1 chondrite and DMM at ca. 485 Ma, 0.124 and 0.121 respectively, these values  
403 range from sub- to slightly supra- chondritic. Intriguingly the highest  $^{187}\text{Os}/^{188}\text{Os}_i$   
404 value was from the most primitive sample: the Black Hill peridotite. The sample of  
405 Truro Volcanics yielded ratios of 0.1825 and 0.1875 and Os concentrations of 17.642  
406 and 18.190 ppt in duplicate analyses respectively. The Black Hill Peridotite has the  
407 highest Os concentration of 405 ppt, while the granites have Os concentration of  
408 between 0.211 and 0.800 ppt.

409 Proterozoic samples have  $^{187}\text{Os}/^{188}\text{Os}_i$  ratios that range from 0.9467 to 15.71, and  
410 Os concentrations range between 1.40 and 145 ppt, with no obvious correlation. A  
411 clear distinction is observed between Hiltaba A-types that exhibit radiogenic initial Os  
412 ratios and relatively high Os concentrations, and Delamerian A-types that exhibit  
413 unradiogenic initial Os ratios and low Os concentrations.

414

415 **Discussion**

416

417 New zircon ages

418

419 The Marcollat Granite age of  $480 \pm 2.5$  Ma is slightly younger than Foden et al.'s  
420 (2006)  $487.1 \pm 1.2$  Ma conventional single zircon age for the same granite. However,  
421 the Mount Monster Porphyry age of  $485.2 \pm 6.9$  Ma overlaps both. A single inherited  
422 concordant zircon dated at  $3034 \pm 58$  Ma represents the first Archean signal detected  
423 in the Delamerian granites. This grain was unlikely to have been assimilated near-  
424 surface, given the absence of an age peak in regional sedimentary zircon data (Ireland  
425 et al., 1998), thus we propose the existence of deep crustal Archean rocks, equivalent  
426 to the  $\sim 3.1$  Ga Cooyerdoo Granite of the eastern Gawler Craton (Fraser et al., 2010)  
427 and/or Archean-derived rocks at significant depth. A single inherited concordant  
428 zircon is dated at  $519 \pm 6$  Ma, which may indicate the Marcollat Granite has interacted  
429 with Truro Volcanics aged material. However, significant crustal contamination to the  
430 granites is ruled out by Os isotope constraints, discussed in a later section.

431

432 Hf isotope constraints

433

434 The maximum recorded  $\epsilon\text{Hf}_i$  of the Marcollat and Mt. Monster samples (+10.4 and  
435 +17.5) approach values for the contemporary depleted MORB mantle (DMM) (Fig.  
436 4). The range (average +4.5, +5.7 respectively) is interpreted to be the result of  
437 complex magma mixing and mingling processes, which is reflected by the  
438 Seismograph Granite whole rock  $\epsilon\text{Hf}_i$  of +3.97. Their source, therefore, is likely to be  
439 mantle, which accounts for the maximum values and also the prevalence of positive  
440 values approaching CHUR. However, the Hf isotope constraints alone do not rule out  
441 crustal contamination.

442 An additional constraint on the degree of crustal contamination in A-type magmas  
443 may be obtained following the approach of Heinonen et al. (2010). These authors  
444 linked magmatic cooling with assimilation of crustal material. Assimilation-related  
445 cooling was inferred by a correlation between decreasing Ti in zircons (lower  
446 temperature, lower Ti concentration; Watson et al., 2006) and less radiogenic Hf  
447 isotopes, as illustrated by figure 5. Assimilation of crust cools the magma, and by the  
448 same processes contributes relatively more-evolved Hf isotopic ratios. Zircons

449 crystallizing during the early stages of this process are predicted to contain relatively  
450 high Ti concentrations and high Hf isotope ratios. Assuming comparable Ti activity  
451 and an isotopically homogeneous assimilant, later zircons must contain relatively less  
452 Ti and lower Hf isotope ratios (see Fig. 5). In our samples, which have not interacted  
453 with crust (see discussion of Os isotopes below), this same approach can be used for a  
454 different purpose – to evaluate the range of initial Hf isotope ratios in the mantle  
455 source.

456 Absolute temperatures for our zircons were not calculated, as the Ti-in-zircon  
457 thermometer is calibrated assuming a rutile —and therefore Ti activity— buffer  
458 (Watson et al., 2006). Since rutile is not observed within the Marcollat or Mt. Monster  
459 samples, we use the measured Ti abundances as a relative guide only. We also include  
460 the caveat that Ti-bearing mineral inclusions within the zircons may introduce a  
461 degree of scatter. To minimise this effect close attention was paid to the signal  
462 quality, to identify spikes that may indicate the presence of an inclusion. However,  
463 evenly distributed micro-inclusions well below the scale of the laser-spot diameter  
464 may present an inherent source of uncertainty (see Pankhurst, 2012).

465 The Mt. Monster zircon population does not suggest a trend (see Fig. 5), and  
466 includes several outliers at high  $^{176}\text{Hf}/^{177}\text{Hf}$ . One interpretation is that these zircons  
467 crystallised ‘early’, prior to crustal assimilation, which suggests the Hf isotope ratios  
468 are a robust reflection of a mantle source. However, these ‘early’ zircons may have  
469 crystallised from a liquid that could have had different Ti activity. Therefore  
470 comparisons between Ti abundance in such zircons are problematic. A cluster of  
471 several analyses is present at high Ti contents, and may well indicate the presence of  
472 Ti-oxide micro-inclusions. Therefore we consider these Ti abundances to  
473 overestimate the real Ti content in the zircons.

474 Ti abundances in the Marcollat zircons show a broad positive correlation with  
475 measured  $^{176}\text{Hf}/^{177}\text{Hf}$  (Fig. 5), which may indicate an assimilation process similar to  
476 that described by Heinonen et al. (2010). However, unlike Heinonen et al.’s (2010)  
477 data that define smooth trends, our data contain many instances of different  
478  $^{176}\text{Hf}/^{177}\text{Hf}$  at similar Ti abundance, as well as many instances of different Ti  
479 abundances with similar  $^{176}\text{Hf}/^{177}\text{Hf}$ . Notwithstanding the possibility of minor  
480 influences from Ti-oxide micro-inclusions, this observation could indicate that mixing  
481 of magmas with different cooling and assimilation histories, each contributed zircons  
482 that record those different magmatic conditions. Since the data in this study spans a



483 range in  $^{176}\text{Hf}/^{177}\text{Hf}_i$  at comparable Ti concentrations, it would seem that no  
484 significant crustal involvement is implied from the Hf data.

485 Mingling of mafic and felsic magmas is observed within the Padthaway Suite —  
486 and indeed in many A-type magmatic systems— most evident where swarms of mafic  
487 enclaves occur within granites and show varying degrees of hybridisation (e.g.  
488 Holden et al., 1991; Turner and Foden, 1996). This causes additional complexities to  
489 the interpretation of whole-rock isotope ratios.

490 Pankhurst et al. (2011c) traced the sources of both mafic enclave and felsic host  
491 within the Delamerian A-type Mannum Granite by conducting in-situ analysis of Nd  
492 isotope ratios within titanite. Those authors demonstrated that while the major and  
493 trace element chemistry is distinct between granite-hosted and enclave-hosted titanite,  
494 isotope ratios are variable outside of analytical error, and the range of initial  
495  $^{143}\text{Nd}/^{144}\text{Nd}$  is similar. One possibility is that a range of sources melted to form  
496 geochemically similar, yet isotopically distinct mafic magmas.

497 The resulting magmas (containing isotopically distinct titanite crystals) were  
498 readily mixed due to similar viscosities. A similar process produced granites  
499 containing chemically similar yet isotopically dissimilar titanite crystals, which also  
500 mixed readily. Mingling occurred between the granite and mafic magmas due to  
501 different viscosities at comparable temperatures (Turner and Foden, 1996). This  
502 model, suggestive of complex, multi-sourced and multi-staged processes could  
503 plausibly result in a wide spread of initial  $^{176}\text{Hf}/^{177}\text{Hf}$  values within zircons, dependent  
504 upon the source of melting, and crystallisation conditions each zircon.

505 Initial Hf isotope ratios from Gawler FLIP samples are range from -1.73 to +4.95.  
506 Crustal contamination is likely to play a limited role in contributing to these isotopic  
507 ratios, since the bulk rock compositions are relatively primitive (46.5 – 53.6 wt%  
508  $\text{SiO}_2$ , 4.43 – 7.1 wt%  $\text{MgO}$ ). The more mafic Gawler FLIP samples contain more  
509 evolved Hf isotope ratios, which suggest their source was also evolved (Fricke, 2005)  
510 relative to depleted mantle, consistent with a plume-like source (e.g. Nelson et al.,  
511 2012). These magmas are consistent with being derived from a plume source as  
512 implied by Betts et al. (2009), but could also originate from enriched lithospheric  
513 mantle, which could also explain their alkalic compositions and Hf isotope ratios  
514 ranging across CHUR.

515 The Hf isotope data from both the Delamerian and Gawler FLIP samples are  
516 suggestive of mantle sources. However, the Delamerian samples contain evidence of

517 appreciably depleted and juvenile material, which has likely mixed with relatively  
518 evolved material, either enriched lithospheric mantle or potentially crustal sources.

519

520 Os isotope constraints

521

522 Os isotopes are particularly distinctive between the A-type rocks of the Delamerian  
523 and Gawler FLIP (see Fig. 6). The  $^{187}\text{Os}/^{188}\text{Os}_i$  of the Delamerian peridotite and felsic  
524 samples are extremely similar, and unradiogenic (Fig 6a). While their total Os  
525 concentrations range over 3 orders of magnitude (0.211 – 405 ppt), their  $^{187}\text{Os}/^{188}\text{Os}_i$   
526 have a comparatively narrow range from 0.1049 to 0.1977. The dramatic difference in  
527 Os concentration is consistent with the ~90% fractionation from a mafic mantle melt  
528 to produce the granitic compositions (Turner et al., 1992). The rhenium-depletion age  
529 of the most unradiogenic sample is  $3.29 \pm 0.4$  Ga. The pre-Delamerian samples (Truro  
530 Volcanics) also contain relatively unradiogenic and homogeneous Os.  $^{187}\text{Os}/^{188}\text{Os}_i$   
531 range from 0.1825 – 0.1875 and concentrations between 1.7 – 1.8 ppt. These ratios  
532 are consistent with a weakly enriched lithospheric mantle source, supporting the  
533 conclusions of Turner et al. (1996a) and Foden et al. (2002a), who describe these  
534 HREE depleted, yet LREE enriched alkali basalts as originating from the upper  
535 lithospheric mantle.

536 Importantly, significant crustal contamination of the Delamerian magmas is ruled  
537 out by the Os data. The concentrations of Os are so low in the granites, that mixing  
538 with any reasonable average crustal component (Fig. 6a) will rapidly produce liquids  
539 that have both Os concentrations and  $^{187}\text{Os}/^{188}\text{Os}_i$  significantly higher than measured  
540 in the Delamerian A-types. In fact, in order to be able to assimilate significant  
541 amounts of crust prior to closed system fractionation, any crustal component requires  
542 anomalously low levels of Os; of the order of sub ppt levels. The extremely low  
543 concentrations of Os and unradiogenic  $^{187}\text{Os}/^{188}\text{Os}_i$  of the felsic samples support a  
544 petrogenesis dominated by closed system fractionation at high crustal levels,  
545 effectively bypassing an evolved lower crustal source.

546 Mt Monster is the only felsic sample which may contain up to a maximum of ~2%  
547 contamination (Fig. 6a) prior to fractionation, and intriguingly, this is the sample that  
548 contains the 3.1 Ga zircon core. The most radiogenic of the Delamerian samples is the  
549 Black Hill Peridotite, which on these models can be accounted for by assimilating a  
550 maximum of 5% crust. Since the Black Hill Peridotite is a significantly larger body

551 than the Marcollat and Seismograph Granites (Turner, 1996), it presumably spent  
552 more time at temperature in the crust, and therefore a greater degree of crustal  
553 assimilation is predicted.

554 Significantly, the other Delamerian samples are subchondritic, and therefore  
555 potentially record heterogeneities in the magma source. Such Os signatures are  
556 confined almost exclusively to the mantle, and therefore we interpret the primary  
557 magmatic source for the Delamerian A-types as the lithospheric mantle with only  
558 minor crustal modification. This is consistent with the conclusions of Foden et al.  
559 (2002b).

560 In contrast, the Gawler FLIP samples are highly variable and radiogenic  
561 ( $^{187}\text{Os}/^{188}\text{Os}_i$  between 0.9467 and 15.71), and have less variable Os concentrations:  
562 between 11.8 and 145 ppt (Fig. 6b). These ratios clearly demonstrate the magmas' Os  
563 budget was derived from an ancient, evolved source. The high silica end of our  
564 Proterozoic A-type dataset, the Sybella Granite, also contains highly radiogenic Os  
565 ( $^{187}\text{Os}/^{188}\text{Os}_i$  between 2.036 and 4.912), and contains comparatively little Os (1.4 –  
566 1.7 ppt), consistent with fractionation from an Os source similar to that of the Gawler  
567 FLIP.

568 Since prevailing models for the Gawler FLIP invoke a mantle plume genesis (e.g.  
569 Betts et al., 2009), the Os isotopes point clearly towards assimilation of substantial  
570 amounts of continental crust into a plume derived magma. However, since the nature  
571 of the Archaean continental crust is poorly constrained, it is not yet possible to  
572 construct detailed models regarding the relative proportions of such crust. Since the  
573 lithophile isotopes (particularly Nd isotopes) do preserve evidence of a mantle-like  
574 component (Fricke, 2005), it is probable that the Os budget in the assimilated crust  
575 dominates any mantle signature.

576

577 Combined U–Pb, Lu–Hf and Re–Os constraints

578

579 Pankhurst et al. (2011c) found that multiple sources are required to account for the Nd  
580 isotopic variability within a Delamerian A-type granite exhibiting obvious mingling  
581 textures between host granite and mafic enclaves. In our Marcollat Granite- and Mt  
582 Monster Porphyry- examples that lack clear mingling textures, evidence for multiple  
583 sources is demonstrated by the large range of Hf isotope ratios within zircons. Thus  
584 multiple isotopic sources appear to be a feature of this system.

585 The U–Pb data implies a very low level of shallow crustal involvement since only  
586 one of the 68 zircon grains analyzed in this study was clearly inherited, most likely  
587 from a lower crustal source. In addition, the Os isotope data effectively rules out  
588 significant crustal contamination, especially of granites whose Os concentrations are  
589 extremely sensitive to any external source Os.

590 Initial Hf isotope data contains examples of DMM-like ratios, although most  
591 examples are less radiogenic (Fig. 4). Importantly, none are less radiogenic than  
592 CHUR. The spread of initial Hf isotope values appear to be unrelated to  
593 straightforward assimilation of cooler, evolved material (Fig. 5), and since the Os data  
594 rules out crustal contamination (Fig. 6a), this spread is most likely to reflect mantle  
595 source heterogeneity.

596 The sub-chondritic Os values must reflect a lithospheric mantle source, since  
597 contemporary DMM is more radiogenic (see Fig. 6a). The significant heterogeneity of  
598 the source, as required by the spread of Hf data on the positive side of CHUR (Fig. 4),  
599 must therefore have been within the lithospheric mantle. Thus a source dominated by  
600 material from heterogeneous lithospheric mantle is constrained by the combination of  
601 lithophile and chalcophile systems within the Delamerian A-types.

602 The rarity of DMM-like Hf isotope ratios recorded by zircons, and the sub-  
603 chondritic Os isotope ratios argue strongly for a dominant lithospheric mantle source.  
604 The range in both Hf and Os isotope ratios are consistent with a variably enriched and  
605 heterogeneous lithospheric mantle, potentially due to metasomatic processes during  
606 the preceding orogenesis. This interpretation is consistent with both Turner et al.  
607 (1992) and Foden et al. (2002b) who also invoked a metasomatised lithospheric  
608 mantle source for the Delamerian A-types on the basis of major and trace element and  
609 Sr and Nd isotope constraints.

610 Initial Hf isotope ratios from the Gawler FLIP samples are similar to those of the  
611 Delamerian, as they cluster at the radiogenic side of CHUR. In terms of lithophile  
612 elements, both the Gawler FLIP and the Delamerian A-types point to a dominant  
613 mantle component. Such a source for the Gawler province has been suggested on the  
614 basis of high magmatic temperatures (950–1100 °C) and Nd isotopes (Stewart and  
615 Foden, 2001). However, distinct provinciality, reflecting variable and significant  
616 assimilation of crust on a pluton scale has been described (e.g. Swain et al., 2005). In  
617 support of a significant crustal contribution, the initial Os isotope ratios are extremely

618 radiogenic, which can only be reasonably attributed to the involvement of an ancient,  
619 evolved source (Fig. 6b). Assimilation or melting of Archean crust is one possible  
620 explanation, supported by the recent discovery of gneissic Archean granites within the  
621 Gawler Craton (Fraser et al., 2010). Another possibility is the involvement of  
622 metasomatised, highly radiogenic portions of the source region. In either scenario, it  
623 is clear that the Os budget of the Gawler samples are not dominated by an  
624 aesthenospheric mantle signature.

625

626 Do A-type magmas play a role in strengthening lithosphere?

627

628 Granitic magmatism plays an important role in the distribution of heat-producing  
629 elements in the lithosphere, and long-term stability of crustal domains (Sandiford and  
630 McLaren, 2005). The observation that A-type magmas are virtually always post-  
631 kinematic invites speculation as to whether there exists a genetic link between the end  
632 of orogenesis and A-type magmatism on shorter time frames as well. Since the  
633 majority of these post-orogenic magmas remain undeformed, this suggests their  
634 presence within stable crustal domains is not a coincidence. Rather their presence may  
635 be reflective of a strengthening process that either drives or is driven by A-type  
636 magmatism. Removal of heat-producing elements from lithospheric mantle sources  
637 via A-type magmatism may promote the longer-term strength and thus stability of  
638 those source regions.

639 For instance, Puura and Flodén (1999) describe the well-studied 1.65-1.50 Ga  
640 rapakivi magmatism of the Svecofennian Domain as being directly related to crust  
641 thickened by the ~300 Ma older Svecofennian Orogeny. This gravitationally unstable  
642 crust is the driver of mantle diapirism, which causes major crust and mantle melting,  
643 producing the A-type magmas. The magmatism effectively stabilizes the lithospheric  
644 column by resetting the Moho depth and thinning the crust (Puura and Flodén, 1999).

645 Another well-documented example is the Tasmanide orogenies of eastern  
646 Australia, beginning with the Delamerian. A series of eastward-younging orogenies  
647 accreted to then Gondwanan margin, driven by a supra-subduction system. Within  
648 this cyclical amalgamation of continental mass, pulses of mantle input over time are  
649 recorded by positive excursions of Hf and Nd isotope ratios (e.g. DeCelles et al.,  
650 2009) via A-type magmatism that post-date peak deformation of each orogeny (Kemp  
651 et al., 2009). This contrasts with negative Hf and Nd excursions of the syn-orogenic I-

652 and S-type granite record (Kemp et al., 2009). These observations imply the same  
653 process occurred to terminate each of these Phanerozoic orogenies, and promoted  
654 later deformation outboard to continue the cycle. We have progressed the work of  
655 Kemp et al. (2009) to include the Delamerian A-types. Our data definitively establish  
656 that the source of these magmas is a heterogeneous lithospheric mantle. Whole-rock  
657 Os isotope data from the A-types of the subsequent Tasminides would serve as an  
658 authoritative test of whether the same sources were melting at the closing stages of  
659 each orogeny, and therefore the same processes were operating to terminate each  
660 orogeny.

661 Our isotopic evidence from the Delamerian suggests that a heterogeneous  
662 lithospheric mantle was the most important source of the magmas. The magmatic  
663 system produced high-crustal level granites that were ultimately sourced from various  
664 portions of the underlying mantle, representing a significant homogenizing influence  
665 across the lithospheric column. This process may have been driven by convective  
666 removal of orogenic-thickened lithosphere (Turner et al., 1996b), which represents a  
667 fundamental change in the orogenic stress field, terminating the Delamerian Orogeny.  
668 We suggest that the homogenizing influence of the A-type magmatic system  
669 promoted, and potentially drove, local strengthening of this lithosphere via chemical  
670 and therefore physical reorganization/resetting, which directed future deformation  
671 outboard.

672 The decoupling of the Hf and Os isotope systems implies the Gawler FLIP was  
673 produced from a number of sources. Radiogenic initial Nd and Hf isotope ratios  
674 strongly argue for a mantle source, which is consistent with the prevailing plume-  
675 head-arrival model for the province as a whole (Betts et al., 2009). However, an  
676 evolved source must also contribute significant material in order to dominate the Os  
677 budget, which is consistent with the observed skewing of Hf isotope values towards  
678 CHUR. Future work characterizing the Os isotope signature of Gawler Craton crustal  
679 rocks is required to constrain whether the source of the radiogenic Os is crustal, or can  
680 be attributed to highly metasomatised portions of the lithospheric mantle. This  
681 determination has implications for the degree of source heterogeneity within the  
682 Gawler FLIP. In either case, the source of Os is clearly different from that of the  
683 Delamerian samples.

684 The Gawler FLIP contains both mantle and crustal isotopic signatures, which  
685 points to a significant depth range of melting and operation of the magmatic system.

686 The voluminous, high temperature and rapid nature of the GRV emplacement points  
687 to wholesale melting of the fusible portions of the lithospheric column, effectively  
688 homogenizing pre-existing chemical gradients. This, hypothesized, widespread  
689 ‘resetting’ of rheological properties via the A-type magmatism could cause relatively  
690 strengthening of the lithospheric domain, which explains its position as an enduring  
691 stable block today.

692

## 693 **Conclusions**

694

695 The Delamerian and Gawler FLIP A-type systems have numerous similarities. They  
696 share distinctive chemistry and produce bimodal provinces characterized by high  
697 temperature ( $\leq 1100^\circ\text{C}$ ) shallow granites and rheognimbrites/lavas and mid-crustal  
698 mafic intrusions. They both define 1) transient periods of anomalous thermal  
699 gradients, 2) the terminus of their respective orogenies (Delamerian, Wartakan), and  
700 3) have occupied stable lithospheric blocks since. These observations suggest a  
701 common tectono-magmatic process.

702 There are also important differences. The Delamerian system has a comparatively  
703 small total volume, and its architecture is relatively long and narrow. The Gawler  
704 FLIP has a large total volume, and its architecture is elliptical. These features,  
705 independent of chemistry or source, are consistent with normal supra-subduction zone  
706 dynamics producing the Delamerian Orogeny (Kemp et al., 2009), and plume head  
707 involvement in the Gawler FLIP (Betts et al., 2009).

708 Our Hf and Os measurements constrain the dominant source regions of each. The  
709 Delamerian is appreciably depleted, containing DMM like Hf isotope ratios as well as  
710 Os isotope evidence of a lithospheric mantle source. Assimilation of continental crust  
711 plays a minor role, leaving a dominant portion of the signal attributed to  
712 heterogeneous lithospheric mantle. Critically, it is the combined approach of in-situ  
713 Hf analysis and whole rock Os analysis that allow us to confidently rule out crustal  
714 contamination, and instead attribute the range of Hf isotope ratios to be truly  
715 reflective of a heterogeneous lithospheric mantle source.

716 The Gawler FLIP is similarly juvenile in terms of Hf, yet much more evolved in  
717 terms of Os. Partial melting in an ancient lower crust is one explanation for the  
718 extremely radiogenic  $^{187}\text{Os}/^{188}\text{Os}_i$ , although metasomatised portions of a mantle  
719 source may also satisfy the data. Our isotopic data is consistent with widespread

720 melting and significant transfer of material from mantle to crust, caused by the arrival  
721 of a mantle plume head.

722 We observe the same style of magmatism, range of sources and empirical  
723 observation of a stable post-magmatic lithosphere in both the Delamerian and Gawler  
724 FLIP. The geodynamic end-member examples presented here (convective  
725 thinning/plume head arrival) suggest the spectrum of A-type magmatism is indicative  
726 of similar high temperature regimes, which can lead to the strengthening of  
727 lithosphere. If the thermal regime is adequately persistent, coeval fusion of crust and  
728 mantle, resetting of the moho, and removal of heterogeneities is suggested to promote  
729 long-term stability of lithospheric domains.

730

731

### 732 **Acknowledgements**

733

734 Elena Belousova, Will Powell and Rosanna Murphy are thanked for discussions of the  
735 manuscript. Peter Wieland is thanked for laboratory assistance. Bernard Bonin and an  
736 anonymous reviewer are thanked for their constructive comments which improved the  
737 manuscript. MJP would like to thank Karin Barovich, John Clemens and Nigel Harris  
738 for their comments on this manuscript within his PhD thesis. David Hilton is thanked  
739 for his editorial role.

740

741 Figure captions:

742

743 Figure 1. Location and geologic context of samples. a) The Padthaway Suite extends  
744 for ~500 km in a north-northwest direction, parallel with the coastline of southeast  
745 South Australia. The intrusions are exposed by the unroofing of Delamerian orogenic  
746 rocks since ~480 Ma. b) The Gawler Craton, central South Australia, is comprised of  
747 amalgamated Archean, Palaeo- and Mesoproterozoic terranes. The Gawler FLIP  
748 (Allen et al., 2008) represents the final tectono-magmatic event in the central Gawler  
749 Craton, before tectonic and magmatic activity continued on the northern margin  
750 (Stewart and Betts, 2010a).

751

752 Figure 2. Cathodoluminescence images of zircons and analytical spots in this study. a)  
753 Marcollat, b) Mt. Monster Porphyry.



754

755 Figure 3. Age concordia from selected analyses of the a) the Marcollat Granite and b)  
756 the Mt. Monster Porphyry. Discordant data (filled, greyed) were rejected from age  
757 calculations.

758

759 Figure 4. Initial Hf isotope ratios for the Delamerian and Gawler FLIP magmatic  
760 rocks with respect to emplacement age. In both provinces the initial Hf isotope ratios  
761 are more juvenile than CHUR, and a small number of zircons from the Mt. Monster  
762 Porphyry are similar to contemporary DMM. Error bars are smaller than the lines  
763 displayed.

764

765 Figure 5. Measured  $^{176}\text{Hf}/^{177}\text{Hf}$  ratios with respect to Ti concentration. As the Ti-in-  
766 zircon thermobarometer is calibrated using a rutile (and therefore Ti activity) buffer,  
767 and no rutile is observed within the Marcollat Granite or Mt. Monster Porphyry, we  
768 present Ti concentration as a temperature proxy only. Despite scatter due to probable  
769 micro-inclusions of Ti-oxides, a cooling trend can be observed within the Marcollat  
770 data (dashed lines). Mt. Monster Porphyry data is much more scattered and do not  
771 show a meaningful trend.  $^1\text{Zircon}$  data from a biotite granite and a diabase within a  
772 comparable A-type system (Heinonen et al., 2010) are plotted for comparison.  
773 Symbol size is generally larger than the plotted error.

774

775 Figure 6. Initial  $^{187}\text{Os}/^{188}\text{Os}$  ratios against inverse of Os concentration. a) Delamerian  
776 samples occupy a limited range from subchondritic to suprachondritic. The ratios  
777 cannot be explained by crustal assimilation, since mixing between a 10% partial melt  
778 of a DMM source (calculated following the approach of Roy-Barman and Allègre,  
779 1995) and an average crustal component (Os concentration of 100-50 ppt and a  
780  $^{187}\text{Os}/^{188}\text{Os}$  ratio of 10) i) trend to far more radiogenic values than those measured and  
781 ii) do not approach the extremely low concentrations of Os measured. The data are  
782 best explained by closed system fractionation from a depleted lithospheric mantle  
783 source. b) The highly radiogenic values displayed by the Proterozoic samples are  
784 similar to a range of reasonable 3.1 Ga Archean Crustal values, which suggests  
785 mixing between mantle plume components and these ancient rocks could explain our  
786 data. Another possibility is that the high  $^{187}\text{Os}/^{188}\text{Os}$  is due to high Re/Os metasomatic  
787 agents (such as subduction fluids; Widom et al., 1999) present in the source. Future

788 work constraining the Re and Os signature of Gawler basement rocks will allow  
789 meaningful tests of these hypotheses. Error bars are smaller than the symbol size.

790

## 791 **References**

792

793 Allen, S. R., McPhie, J., Ferris, G., and Simpson, C., 2008, Evolution and architecture  
794 of a large felsic Igneous Province in western Laurentia: The 1.6 Ga Gawler  
795 Range Volcanics, South Australia: *Journal of Volcanology and Geothermal*  
796 *Research*, v. 172, no. 1-2, p. 132-147.

797 Allen, S. R., Simpson, C. J., McPhie, J., and Daly, S. J., 2003, Stratigraphy,  
798 distribution and geochemistry of widespread felsic volcanic units in the  
799 Mesoproterozoic Gawler Range Volcanics, South Australia: *Australian*  
800 *Journal of Earth Sciences*, v. 50, no. 1, p. 97-112.

801 Arroucau, P., Rawlinson, N., and Sambridge, M., 2010, New insight into Cainozoic  
802 sedimentary basins and Palaeozoic suture zones in southeast Australia from  
803 ambient noise surface wave tomography: *Geophys. Res. Lett.*, v. 37, p.  
804 L07303.

805 Belousova, E., Griffin, W. L., O'Reilly, S. Y., and Fisher, N. I., 2002, Igneous zircon:  
806 trace element composition as an indicator of source rock type: *Contributions*  
807 *to Mineralogy and Petrology*, v. 143, no. 5, p. 602-622.

808 Belousova, E. A., Griffin, W. L., and O'Reilly, S. Y., 2006, Zircon Crystal  
809 Morphology, Trace Element Signatures and Hf Isotope Composition as a Tool  
810 for Petrogenetic Modelling: Examples From Eastern Australian Granitoids:  
811 *Journal of Petrology*, v. 47, no. 2, p. 329-353.

812 Belousova, E. A., Reid, A. J., Griffin, W. L., and O'Reilly, S. Y., 2009, Rejuvenation  
813 vs. recycling of Archean crust in the Gawler Craton, South Australia:  
814 Evidence from U-Pb and Hf isotopes in detrital zircon: *Lithos*, v. 113, no. 3-4,  
815 p. 570-582.

816 Betts, P. G., and Giles, D., 2006, The 1800-1100 Ma tectonic evolution of Australia:  
817 *Precambrian Research*, v. 144, p. 92-125.

818 Betts, P. G., Giles, D., Foden, J., Schaefer, B. F., Mark, G., Pankhurst, M. J., Forbes,  
819 C. J., Williams, H. A., Chalmers, N. C., and Hills, Q., 2009, Mesoproterozoic  
820 plume-modified orogenesis in eastern Precambrian Australia: *Tectonics*, v. 28,  
821 p. Tc3006.

822 Betts, P. G., Giles, D., Lister, G. S., and Frick, L. R., 2002, Evolution of the  
823 Australian lithosphere: *Australian Journal of Earth Sciences*, v. 49, no. 4, p.  
824 661-695.

825 Betts, P. G., Giles, D., Schaefer, B. F., and Mark, G., 2007, 1600–1500 Ma hotspot  
826 track in eastern Australia: implications for Mesoproterozoic continental  
827 reconstructions: *Terra Nova*, v. 19, no. 6, p. 496-501.

828 Betts, P. G., Mason, W. G., and Moresi, L., 2012, The influence of a mantle plume  
829 head on the dynamics of a retreating subduction zone: *Geology*, v. 40, no. 8, p.  
830 739-742.

831 Blichert-Toft, J., and Albarède, F., 1997, The Lu-Hf isotope geochemistry of  
832 chondrites and the evolution of the mantle-crust system: *Earth and Planetary*  
833 *Science Letters*, v. 148, no. 1-2, p. 243-258.

834 Blissett, A. H., Creaser, R. A., Daly, S. J., Flint, R. B., and Parker, A. J., 1993,  
835 Gawler Range Volcanics, *in* Drexel, J. F., Preiss, W. V., and Parker, A. J.,

836 eds., *The geology of South Australia, Volume 1: The Precambrian*: Adelaide,  
837 Department of Mines and Energy, p. 106-124.

838 Bonin, B., 2007, A-type granites and related rocks: Evolution of a concept, problems  
839 and prospects: *Lithos*, v. 97, no. 1-2, p. 1-29.

840 Clemens, J. D., Holloway, J. R., and White, A. J. R., 1986, Origin of an A-type  
841 granite; experimental constraints: *American Mineralogist*, v. 71, no. 3-4, p.  
842 317-324.

843 Collins, W., Beams, S., White, A., and Chappell, B., 1982, Nature and origin of A-  
844 type granites with particular reference to southeastern Australia: *Contributions*  
845 *to Mineralogy and Petrology*, v. 80, no. 2, p. 189-200.

846 Creaser, R. A., 1995, Neodymium isotopic constraints for the origin of  
847 Mesoproterozoic silicic magmatism, Gawler Craton, South Australia.:  
848 *Canadian Journal of Earth Sciences*, v. 32, p. 469-471.

849 Creaser, R. A., and Fanning, C. M., 1993, A U-Pb Zircon Study of the  
850 Mesoproterozoic Charleston Granite, Gawler Craton, South-Australia:  
851 *Australian Journal of Earth Sciences*, v. 40, no. 6, p. 519-526.

852 Creaser, R. A., Price, R. C., and Wormald, R. J., 1991, A-type granites revisited:  
853 Assessment of a residual-source model: *Geology*, v. 19, no. 2, p. 163-166.

854 Dall'Agnol, R., Frost, C. D., and Rämö, O. T., 2012, IGCP Project 510 "A-type  
855 Granites and Related Rocks through Time" Project vita, results, and  
856 contribution to granite research: *Lithos*, v. 151, no. 0, p. 1-16.

857 Dargahi, S., Arvin, M., Pan, Y. M., and Babaei, A., 2010, Petrogenesis of post-  
858 collisional A-type granitoids from the Urumieh-Dokhtar magmatic  
859 assemblage, Southwestern Kerman, Iran: Constraints on the Arabian-Eurasian  
860 continental collision: *Lithos*, v. 115, no. 1-4, p. 190-204.

861 DeCelles, P. G., Ducea, M. N., Kapp, P., and Zandt, G., 2009, Cyclicity in Cordilleran  
862 orogenic systems: *Nature Geoscience*, v. 2, no. 4, p. 251-257.

863 DePaolo, D. J., 1981, Trace element and isotopic effects of combined wallrock  
864 assimilation and fractional crystallization: *Earth and Planetary Science Letters*,  
865 v. 53, no. 2, p. 189-202.

866 Eby, G. N., 1992, Chemical subdivision of the A-type granitoids: Petrogenetic and  
867 tectonic implications: *Geology*, v. 20, no. 7, p. 641-644.

868 Elhlou, S., Belousova, E. A., Griffin, W. L., Pearson, N. J., and O'Reilly, S. Y., 2006,  
869 Trace element and isotopic composition of GJ red zircon standard by laser  
870 ablation: *Geochimica et Cosmochimica Acta*, v. 70, no. 18, p. A158.

871 Fanning, C. M., Flint, R. B., Parker, A. J., Ludwig, K. R., and Blissett, A. H., 1988,  
872 Refined Proterozoic evolution of the Gawler Craton, South Australia, through  
873 U-Pb zircon geochronology: *Precambrian Research*, v. 40-41, p. 363-386.

874 Flint, R. B., 1993, Mesoproterozoic, *in* Drexel, J. F., Preiss, W. V., and Parker, A. J.,  
875 eds., *The Geology of South Australia, vol. 1: The Precambrian, Volume*  
876 *Bulletin 54, Geol. Surv. South Australia*, p. 107-169.

877 Foden, J., Elburg, M. A., Dougherty-Page, J., and Burt, A., 2006, The Timing and  
878 Duration of the Delamerian Orogeny: Correlation with the Ross Orogen and  
879 Implications for Gondwana Assembly: *The Journal of Geology*, v. 114, no. 2,  
880 p. 189-210.

881 Foden, J., Song, S. H., Turner, S., Elburg, M., Smith, P. B., Van der Steldt, B., and  
882 Van Penglis, D., 2002a, Geochemical evolution of lithospheric mantle beneath  
883 S.E. South Australia: *Chemical Geology*, v. 182, no. 2-4, p. 663-695.

884 Foden, J. D., Elburg, M. A., Turner, S. P., Sandiford, M., O'Callaghan, J., and  
885 Mitchell, S., 2002b, Granite production in the Delamerian Orogen, South  
886 Australia: *Journal of the Geological Society*, v. 159, p. 557-575.

887 Forbes, B. G., Coates, R. P., and Daily, B., 1972, Truro Volcanics: Quarterly  
888 geological notes. *Geol. Surv. South Aust.*, v. 44, p. 1-5.

889 Fraser, G., McAvaney, S., Neumann, N., Szpunar, M., and Reid, A., 2010, Discovery  
890 of early Mesoarchean crust in the eastern Gawler Craton, South Australia:  
891 *Precambrian Research*, v. 179, no. 1, p. 1-21.

892 Fricke, C., 2005, Source and origin of the lower Gawler Range Volcanics, (GRV),  
893 South Australia: geochemical constraints from mafic magmas., Monash  
894 University.

895 Frost, A. M., 2009, Petrogenesis, Modelling and Characterisation of Layered Mafic  
896 Intrusion White Hill and Peculiar Knob North within the Mount Woods Inlier,  
897 South Australia [Honours: Macquarie University].

898 Frost, C. D., and Frost, B. R., 1997, Reduced rapakivi-type granites: The tholeiite  
899 connection: *Geology*, v. 25, no. 7, p. 647-650.

900 Goodge, J. W., and Vervoort, J. D., 2006, Origin of Mesoproterozoic A-type granites  
901 in Laurentia: Hf isotope evidence: *Earth and Planetary Science Letters*, v. 243,  
902 p. 711-731.

903 Gregory, M. J., Schaefer, B. F., Keays, R. R., and Wilde, A. R., 2008, Re-Os  
904 systematics of the Mt Isa copper ore body and the Eastern Creek Volcanics,  
905 Queensland, Australia: *Mineralium Deposita*, v. 43, p. 553-573.

906 Heinonen, A. P., Andersen, T., and Rämö, O. T., 2010, Re-evaluation of Rapakivi  
907 Petrogenesis: Source Constraints from the Hf Isotope Composition of Zircon  
908 in the Rapakivi Granites and Associated Mafic Rocks of Southern Finland:  
909 *Journal of Petrology*, v. 51, no. 8, p. 1687-1709.

910 Holden, P., Halliday, A. N., Stephens, W. E., and Henney, P. J., 1991, Chemical and  
911 Isotopic Evidence for Major Mass-Transfer between Mafic Enclaves and  
912 Felsic Magma: *Chemical Geology*, v. 92, no. 1-3, p. 135-152.

913 Homburg, J. M., Hirth, G., and Kelemen, P. B., 2010, Investigation of the strength  
914 contrast at the Moho: A case study from the Oman Ophiolite: *Geology*, v. 38,  
915 no. 8, p. 679-682.

916 Huang, H.-Q., Li, X.-H., Li, W.-X., and Li, Z.-X., 2011, Formation of high  $\delta^{18}\text{O}$   
917 fayalite-bearing A-type granite by high-temperature melting of granulitic  
918 metasedimentary rocks, southern China: *Geology*, v. 39, no. 10, p. 903-906.

919 Ireland, T. R., Flöttmann, T., Fanning, C. M., Gibson, G. M., and Preiss, W. V., 1998,  
920 Development of the early Paleozoic Pacific margin of Gondwana from  
921 detrital-zircon ages across the Delamerian orogen: *Geology*, v. 26, no. 3, p.  
922 243-246.

923 Jackson, S. E., Pearson, N. J., Griffin, W. L., and Belousova, E. A., 2004, The  
924 application of laser ablation-inductively coupled plasma-mass spectrometry to  
925 in situ U-Pb zircon geochronology: *Chemical Geology*, v. 211, no. 1-2, p. 47-  
926 69.

927 Johnson, C. M., Shirey, S. B., and Barovich, K. M., 1996, New approaches to crustal  
928 evolution studies and the origin of granitic rocks: what can the Lu-Hf and Re-  
929 Os isotope systems tell us?: *Earth and Environmental Science Transactions of*  
930 *the Royal Society of Edinburgh*, v. 87, no. 1-2, p. 339-352.

931 Kelemen, P. B., and Dick, H. J. B., 1995, Focused melt flow and localized  
932 deformation in the upper mantle: Juxtaposition of replacive dunite and ductile

933 shear zones in the Josephine peridotite, SW Oregon: *Journal of Geophysical*  
934 *Research*, v. 100, no. B1.

935 Kelemen, P. B., and Hirth, G., 2007, A periodic shear-heating mechanism for  
936 intermediate-depth earthquakes in the mantle: *Nature*, v. 446, p. 787-790.

937 Kemp, A. I. S., Hawkesworth, C. J., Collins, W. J., Gray, C. M., and Blevin, P. L.,  
938 2009, Isotopic evidence for rapid continental growth in an extensional  
939 accretionary orogen: The Tasmanides, eastern Australia: *Earth and Planetary*  
940 *Science Letters*, v. 284, no. 3-4, p. 455-466.

941 Kennedy, R. J., 1989, A 3D gravity and aeromagnetic interpretation of the Black Hill-  
942 Cambrai Region [Honours: University of Adelaide].

943 King, P. L., Chappell, B. W., Allen, C. M., and White, A. J. R., 2001, Are A-type  
944 granites the high-temperature felsic granites? Evidence from fractionated  
945 granites of the Wangrah Suite: *Australian Journal of Earth Sciences*, v. 48, no.  
946 4, p. 501-514.

947 Loiselle, M. C., and Wones, D. R., Characteristics and origin of anorogenic granites, *in*  
948 *Proceedings Geol Soc Am Abstr with Progr* 1979, Volume 11, p. 468.

949 Menuge, J. F., Brewer, T. S., and Seeger, C. M., 2002, Petrogenesis of metaluminous  
950 A-type rhyolites from the St Francois Mountains, Missouri and the  
951 Mesoproterozoic evolution of the southern Laurentian margin: *Precambrian*  
952 *Research*, v. 113, no. 3-4, p. 269-291.

953 Nelson, W. R., Furman, T., van Keken, P. E., Shirey, S. B., and Hanan, B. B., 2012,  
954 OsHf isotopic insight into mantle plume dynamics beneath the East African  
955 Rift System: *Chemical Geology*, v. 320-321, no. 0, p. 66-79.

956 Paczkowski, K., Bercovici, D., Landuyt, W., and Brandon, M. T., 2012, Drip  
957 instabilities of continental lithosphere: acceleration and entrainment by  
958 damage: *Geophysical Journal International*, v. 189, no. 2, p. 717-729.

959 Pankhurst, M. J., 2012, Determining the source of post-orogenic magmatism to  
960 constrain terminal orogenesis. [PhD (unpublished): Macquarie University].

961 Pankhurst, M. J., Schaefer, B. F., and Betts, P. G., 2011a, Geodynamics of rapid  
962 voluminous felsic magmatism through time: *Lithos*, v. 123, p. 92-101.

963 Pankhurst, M. J., Schaefer, B. F., Betts, P. G., Phillips, N., and Hand, M., 2011b, A  
964 Mesoproterozoic continental flood rhyolite province, the Gawler Ranges,  
965 Australia: the end member example of the Large Igneous Province clan: *Solid*  
966 *Earth*, v. 2, p. 1-9.

967 Pankhurst, M. J., Vernon, R. H., Turner, S. P., Schaefer, B. F., and Foden, J., 2011c,  
968 Contrasting Sr and Nd isotopic behaviour during magma mingling; new  
969 insights from the Mannum A-type granite: *Lithos*, v. 126, p. 135-146.

970 Phillips, N., 2006, Geophysical modeling of the Hutchison Group beneath the Gawler  
971 Range Volcanics, Gawler Craton, South Australia [Honours: Monash  
972 University].

973 Platt, J. P., and Behr, W. M., 2011, Grainsize evolution in ductile shear zones:  
974 Implications for strain localization and the strength of the lithosphere: *Journal*  
975 *of Structural Geology*, v. 33, no. 4, p. 537-550.

976 Puura, V., and Flodén, T., 1999, Rapakivi-granite-anorthosite magmatism - a way of  
977 thinning and stabilisation of the Svecofennian crust, Baltic Sea Basin:  
978 *Tectonophysics*, v. 305, no. 1-3, p. 75-92.

979 Rajagopalan, S., Zhiqun, S., and Major, R., 1993, Geophysical investigations of  
980 volcanic terrains: A case history from the Gawler Range Volcanic Province,  
981 South Australia: *Exploration Geophysics*, v. 24, p. 769-778.

- 982 Rämö, O. T., and Haapala, I., 1995, One hundred years of rapakivi granite:  
983 Mineralogy and Petrology, v. 52, no. 3-4, p. 129-185.
- 984 Rocchi, S., Di Vincenzo, G., Ghezzo, C., and Nardini, I., 2009, Granite-lamprophyre  
985 connection in the latest stages of the early Paleozoic Ross Orogeny (Victoria  
986 Land, Antarctica): Bulletin of the Geological Society of America, v. 121, no.  
987 5-6, p. 801-819.
- 988 Roy-Barman, M., and Allègre, C. J., 1995,  $^{187}\text{Os}/^{186}\text{Os}$  in oceanic island basalts:  
989 tracing oceanic crust recycling in the mantle: Earth and Planetary Science  
990 Letters, v. 129, no. 1, p. 145-161.
- 991 Rutanen, H., Andersson, U. B., Väisänen, M., Johansson, A., Fröjdö, S., Lahaye, Y.,  
992 and Eklund, O., 2010, 1.8 Ga magmatism in southern Finland: strongly  
993 enriched mantle and juvenile crustal sources in a post-collisional setting:  
994 International Geology Review, v. 53, no. 14, p. 1622-1683.
- 995 Sandiford, M., and McLaren, S., 2005, Thermo-mechanical controls on heat  
996 production element distributions and the long term evolution of the  
997 continentents., in Brown, M., and Rushmer, T., eds., Evolution and  
998 Differentiation of the Continental Crust, Cambridge University Press, p. 67-  
999 91.
- 1000 Schaefer, B. F., Pearson, D. G., Rogers, N. W., and Barnicoat, A. C., 2010, Re- $\text{Os}$   
1001 isotope and PGE constraints on the timing and origin of gold mineralisation in  
1002 the Witwatersrand Basin: Chemical Geology, v. 276, no. 1, p. 88-94.
- 1003 Schaefer, B. F., Turner, S. P., Rogers, N. W., Hawkesworth, C. J., Williams, H. M.,  
1004 Pearson, G. D., and Nowell, G. M., 2000, Re-Os isotope characteristics of  
1005 postorogenic lavas: Implications for the nature of young lithospheric mantle  
1006 and its contribution to basaltic magmas: Geology, v. 28, no. 6, p. 563-566.
- 1007 Shellnutt, J. G., and Zhou, M.-F., 2007, Permian peralkaline, peraluminous and  
1008 metaluminous A-type granites in the Panxi district, SW China: Their  
1009 relationship to the Emeishan mantle plume: Chemical Geology, v. 243, p. 286-  
1010 316.
- 1011 Shirey, S. B., and Walker, R. J., 1995, Carius tube digestion for low-blank rhenium-  
1012 osmium analysis.: Analytical Chemistry, v. 67, p. 2136-2141.
- 1013 -, 1998, The Re-Os isotope system in cosmochemistry and high-temperature  
1014 geochemistry: Annual Review of Earth and Planetary Sciences, v. 26, p. 423-  
1015 500.
- 1016 Siguigna, A. P., Larabee, A. J., and Waddington, J. C., 1982, The half life of  $^{176}\text{Lu}$  by  
1017 a  $\gamma$ - $\gamma$  coincidence measurement: Can. J. Phys., v. 60, p. 361-364.
- 1018 Stewart, J. R., and Betts, P. G., 2010a, Late Paleo-Mesoproterozoic plate margin  
1019 deformation in the southern Gawler Craton: Insights from structural and  
1020 aeromagnetic analysis: Precambrian Research, v. 177, no. 1, p. 55-72.
- 1021 Stewart, J. R., and Betts, P. G., 2010b, Late Paleo-Mesoproterozoic plate margin  
1022 deformation in the southern Gawler Craton: Insights from structural and  
1023 aeromagnetic analysis: Precambrian Research, v. 177, p. 55-72.
- 1024 Stewart, K. P., 1994, High temperature felsic volcanism and the role of mantle  
1025 magmas in Proterozoic Crustal growth [PhD: Adelaide University].
- 1026 Stewart, K. P., and Foden, J., 2001, Mesoproterozoic granitoids of South Australia:  
1027 Part 1 Ð the Gawler Craton: University of Adelaide (unpublished).
- 1028 Sundberg, M., Hirth, G., and Kelemen, P. B., 2010, Trapped Melt in the Josephine  
1029 Peridotite: Implications for Permeability and Melt Extraction in the Upper  
1030 Mantle: Journal of Petrology, v. 51, no. 1-2, p. 185-200.

- 1031 Swain, G., Barovich, K., Hand, M., Ferris, G., and Schwarz, M., 2008, Petrogenesis  
1032 of the St Peter Suite, southern Australia: Arc magmatism and Proterozoic  
1033 crustal growth of the South Australian Craton: *Precambrian Research*, v. 166,  
1034 p. 283-296.
- 1035 Swain, G., Woodhouse A., Hand, M., Barovich, K., Schwarz, M., and Fanning, C. M.,  
1036 2005, Provenance and tectonic development of the late Archean Gawler  
1037 Craton, Australia; U-Pb zircon, geochemical and Sm-Nd isotopic implications:  
1038 *Precambrian Research*, v. 141, p. 106-136.
- 1039 Turner, S., Arnaud, N., Liu, J., Rogers, N., Hawkesworth, C., Harris, N., Kelley, S.,  
1040 Van Calsteren, P., and Deng, W., 1996a, Post-collision, Shoshonitic  
1041 Volcanism on the Tibetan Plateau: Implications for Convective Thinning of  
1042 the Lithosphere and the Source of Ocean Island Basalts: *Journal of Petrology*,  
1043 v. 37, no. 1, p. 45-71.
- 1044 Turner, S., and Foden, J., 1996, Magma mingling in late-Delamerian A-type granites  
1045 at Mannum, south Australia: *Mineralogy and Petrology*, v. 56, no. 3-4, p. 147-  
1046 169.
- 1047 Turner, S. P., 1996, Petrogenesis of the late-Delamerian gabbroic complex at Black  
1048 Hill, South Australia: Implications for convective thinning of the lithospheric  
1049 mantle: *Mineralogy and Petrology*, v. 56, no. 1, p. 51-89.
- 1050 Turner, S. P., and Foden, J., 1990, The nature of mafic magmatism through the  
1051 development of the Adelaide Geosyncline and the subsequent Delamerian  
1052 Orogeny, South Australia., *in* Parker, A. J., Rickwood, P. C., and Tucker, D.  
1053 H., eds., *Mafic Dykes and Emplacement Mechanisms*: Rotterdam, A. A.  
1054 Balkema, p. 431-434.
- 1055 Turner, S. P., Foden, J. D., and Morrison, R. S., 1992, Derivation of Some A-Type  
1056 Magmas by Fractionation of Basaltic Magma - an Example from the  
1057 Padthaway Ridge, South Australia: *Lithos*, v. 28, no. 2, p. 151-179.
- 1058 Turner, S. P., Kelley, S. P., VandenBerg, A. H. M., Foden, J. D., Sandiford, M., and  
1059 Flottmann, T., 1996b, Source of the Lachlan fold belt flysch linked to  
1060 convective removal of the lithospheric mantle and rapid exhumation of the  
1061 Delamerian-Ross fold belt: *Geology*, v. 24, no. 10, p. 941-944.
- 1062 Turner, S. P., and Rushmer, T., 2009, Similarities between mantle-derived A-type  
1063 granites and voluminous rhyolites in continental flood basalts provinces: *Earth  
1064 and Environmental Science Transactions of the Royal Society of Edinburgh*, v.  
1065 100, p. 1-10.
- 1066 Villaseca, C., Orejana, D., and Belousova, E. A., 2012, Recycled metaigneous crustal  
1067 sources for S- and I-type Variscan granitoids from the Spanish Central System  
1068 batholith: Constraints from Hf isotope zircon composition: *Lithos*, v. 153, p.  
1069 84-93.
- 1070 Vissers, R. L. M., Drury, M. R., Hoogerduijn, Strating, E. H., Spiers, C. J., and van  
1071 der Wal, D., 1995, Mantle shear zones and their effect on lithosphere strength  
1072 during continental breakup: *Tectonophysics*, v. 249, no. 3-4, p. 155-171.
- 1073 Wade, B. P., Barovich, K. M., Hand, M., Scrimgeour, I. R., and Close, D. F., 2006,  
1074 Evidence for Early Mesoproterozoic Arc Magmatism in the Musgrave Block,  
1075 Central Australia: Implications for Proterozoic Crustal Growth and Tectonic  
1076 Reconstructions of Australia: *Journal of Geology*, v. 114, no. 1, p. 43-63.
- 1077 Watson, E., Wark, D., and Thomas, J., 2006, Crystallization thermometers for zircon  
1078 and rutile: *Contributions to Mineralogy and Petrology*, v. 151, no. 4, p. 413-  
1079 433.

- 1080 Whalen, J. B., Currie, K. L., and Chappell, B. W., 1987, A-type granites; geochemical  
1081 characteristics, discrimination and petrogenesis: *Contributions to Mineralogy*  
1082 and *Petrology*, v. 95, no. 4, p. 407-419.
- 1083 Widom, E., Hoernle, K. A., Shirey, S. B., and Schmincke, H.-U., 1999, Os Isotope  
1084 Systematics in the Canary Islands and Madeira: Lithospheric Contamination  
1085 and Mantle Plume Signatures: *Journal of Petrology*, v. 40, no. 2, p. 279-296.  
1086  
1087



Figure 1a

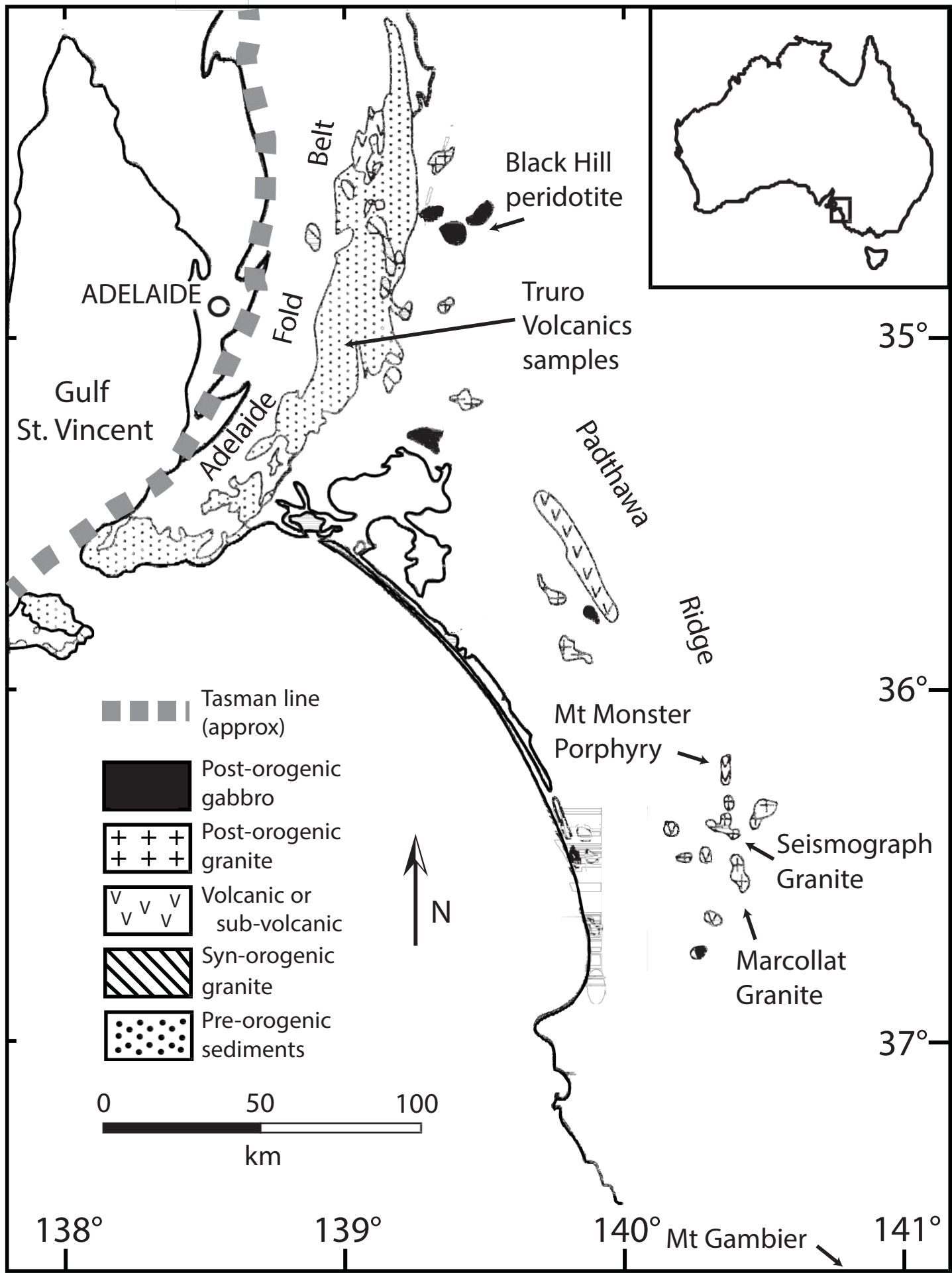


Figure 1b

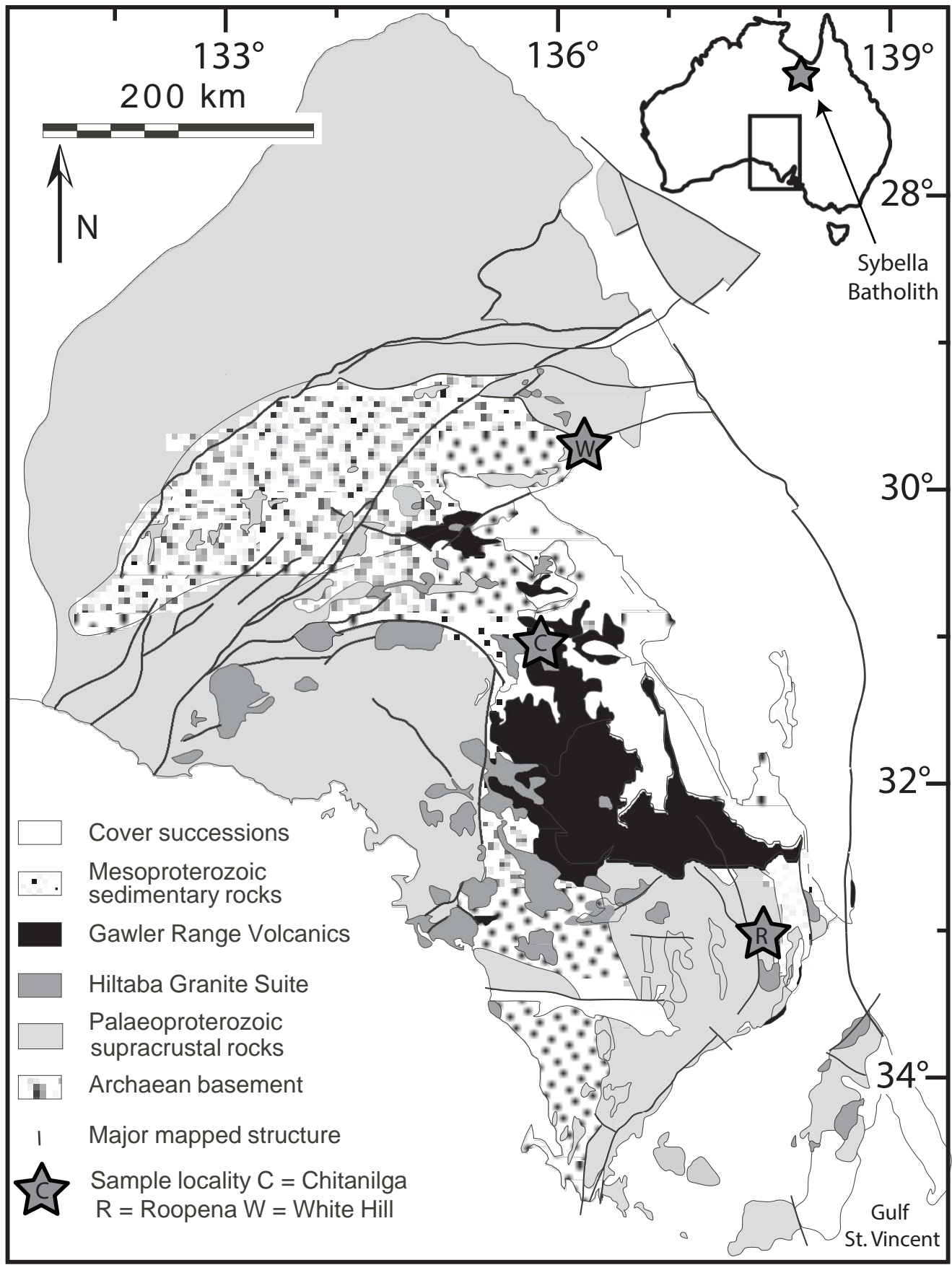


Figure 3a

Figure 3a

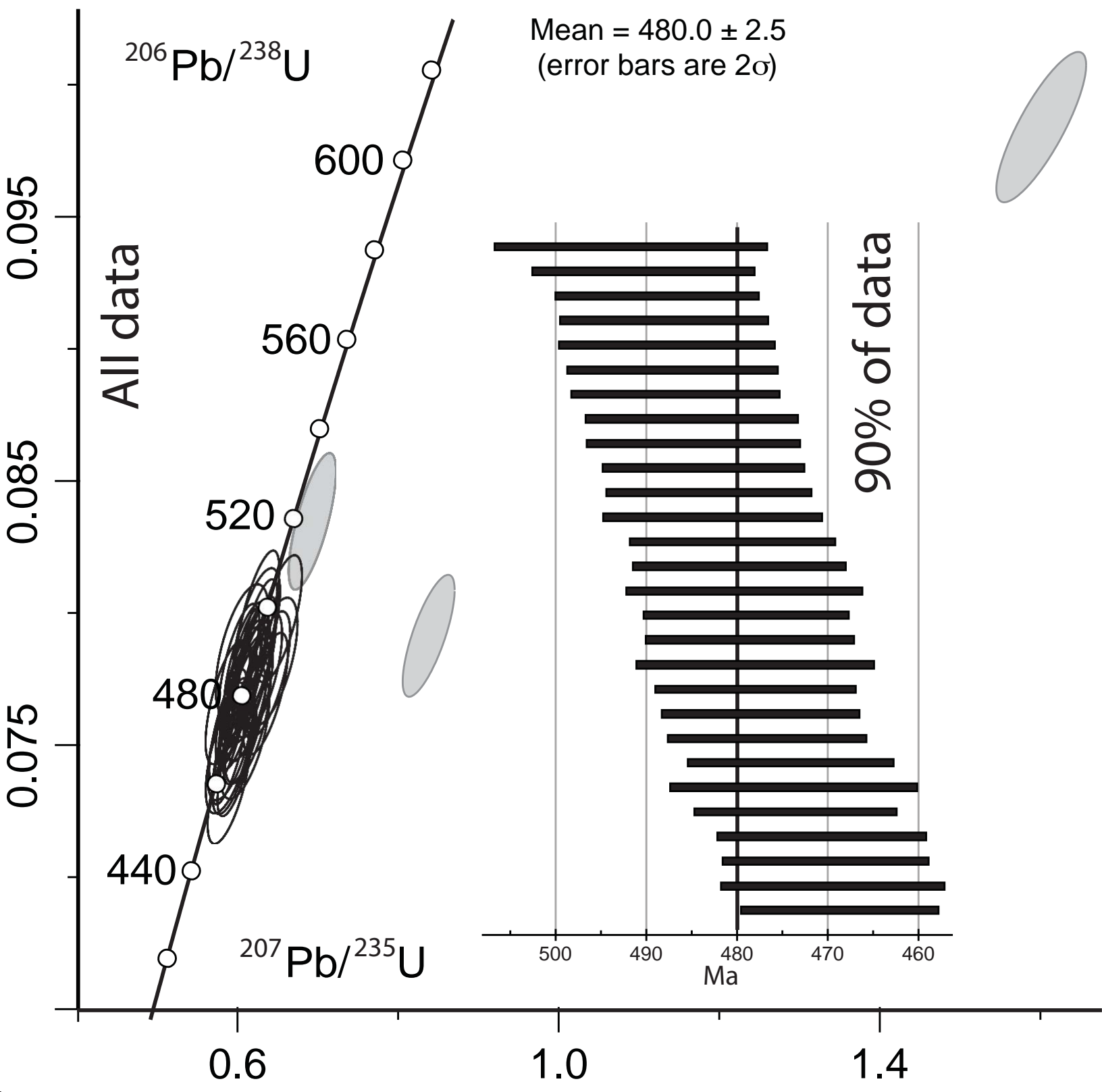


Figure 3b

Figure 3b

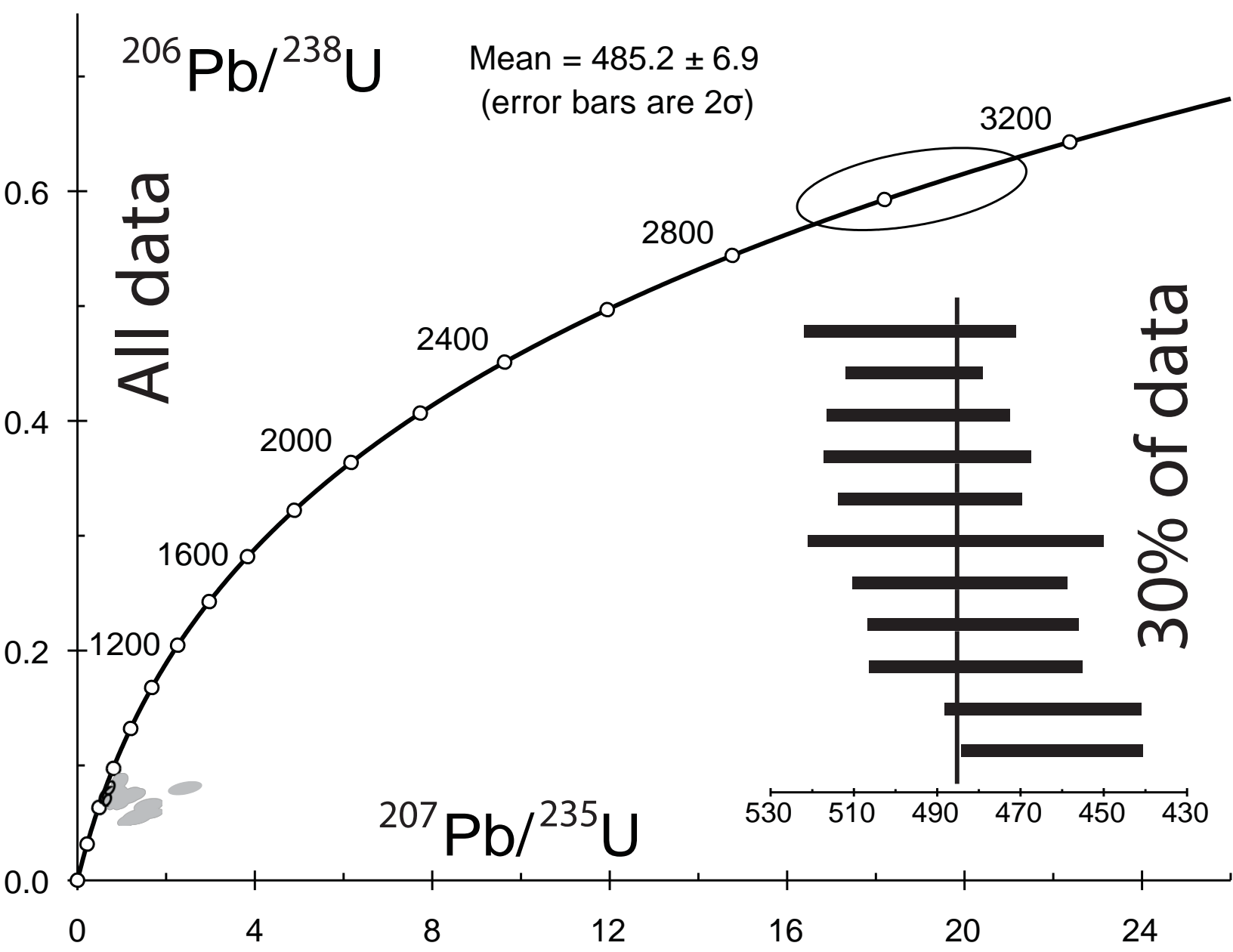


Figure 4

Figure 4

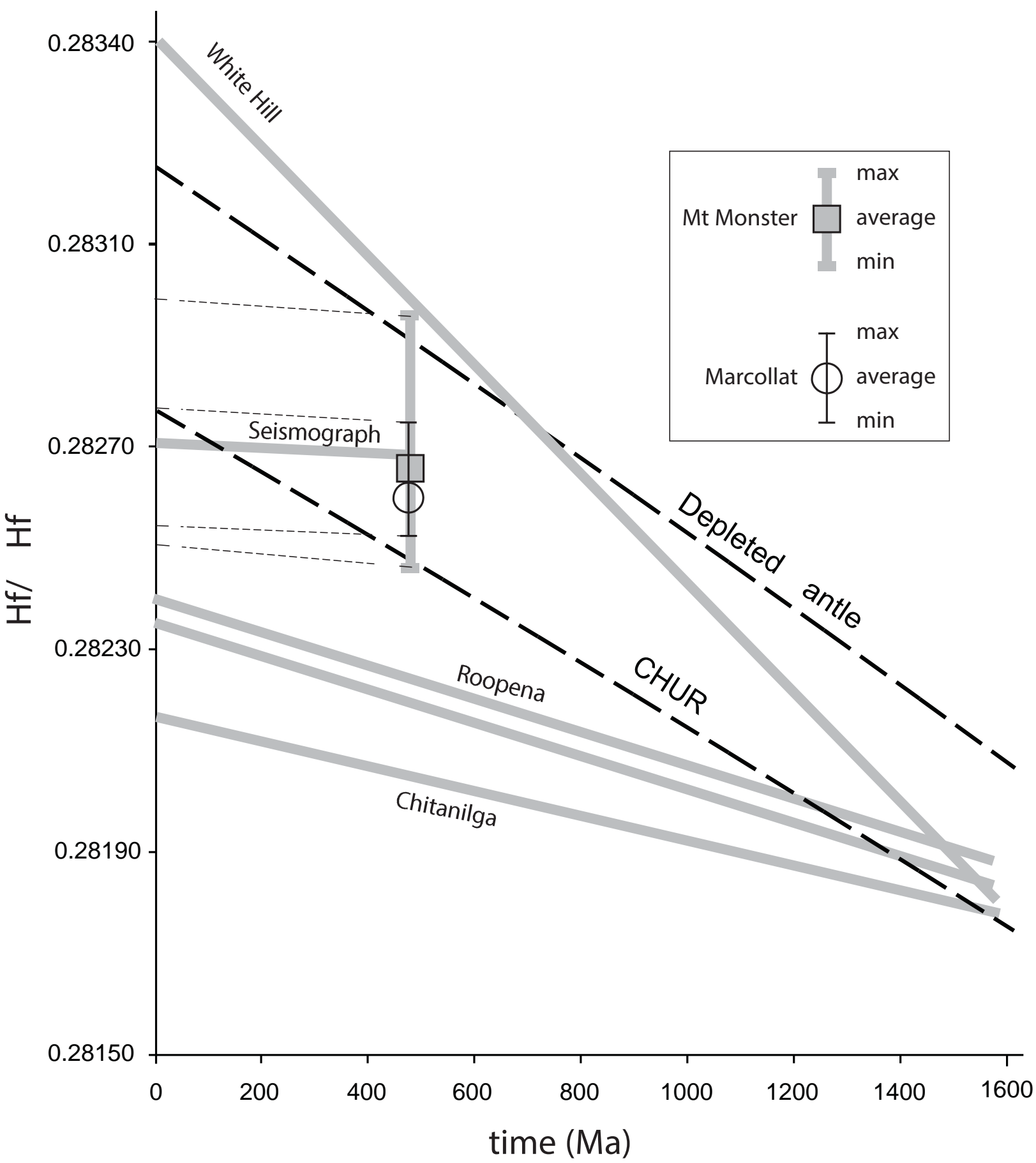


Figure 5

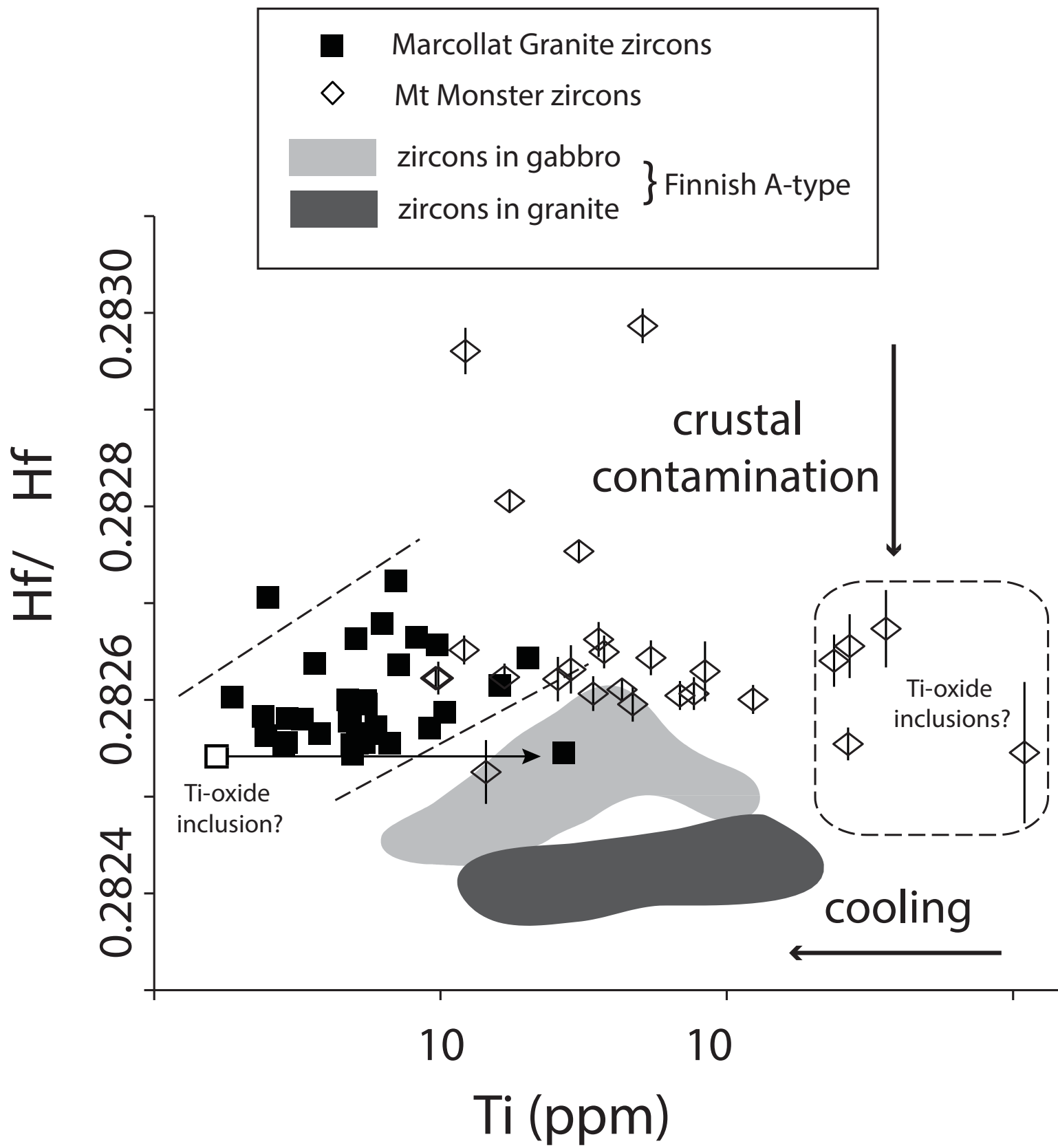


Figure 2a

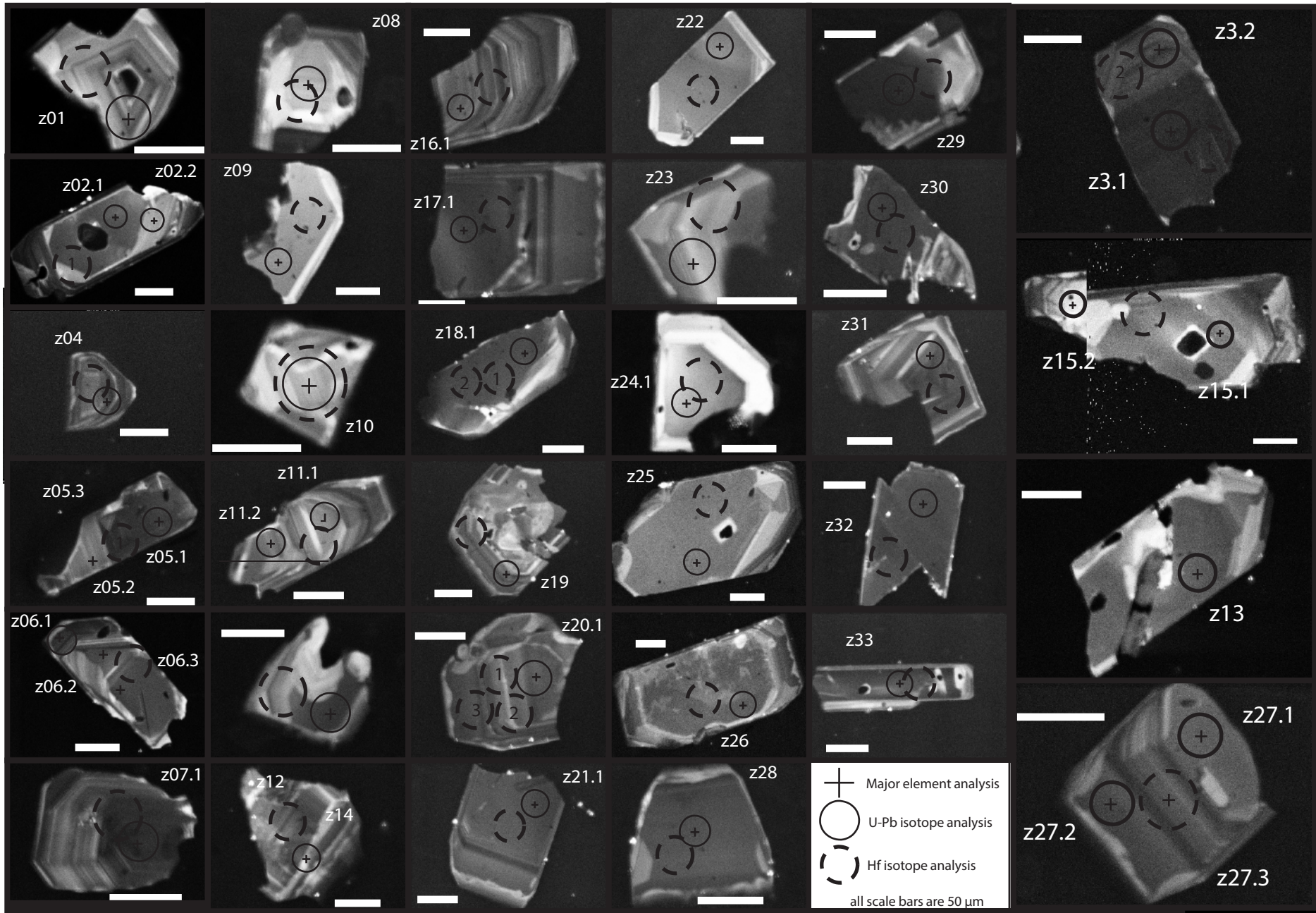
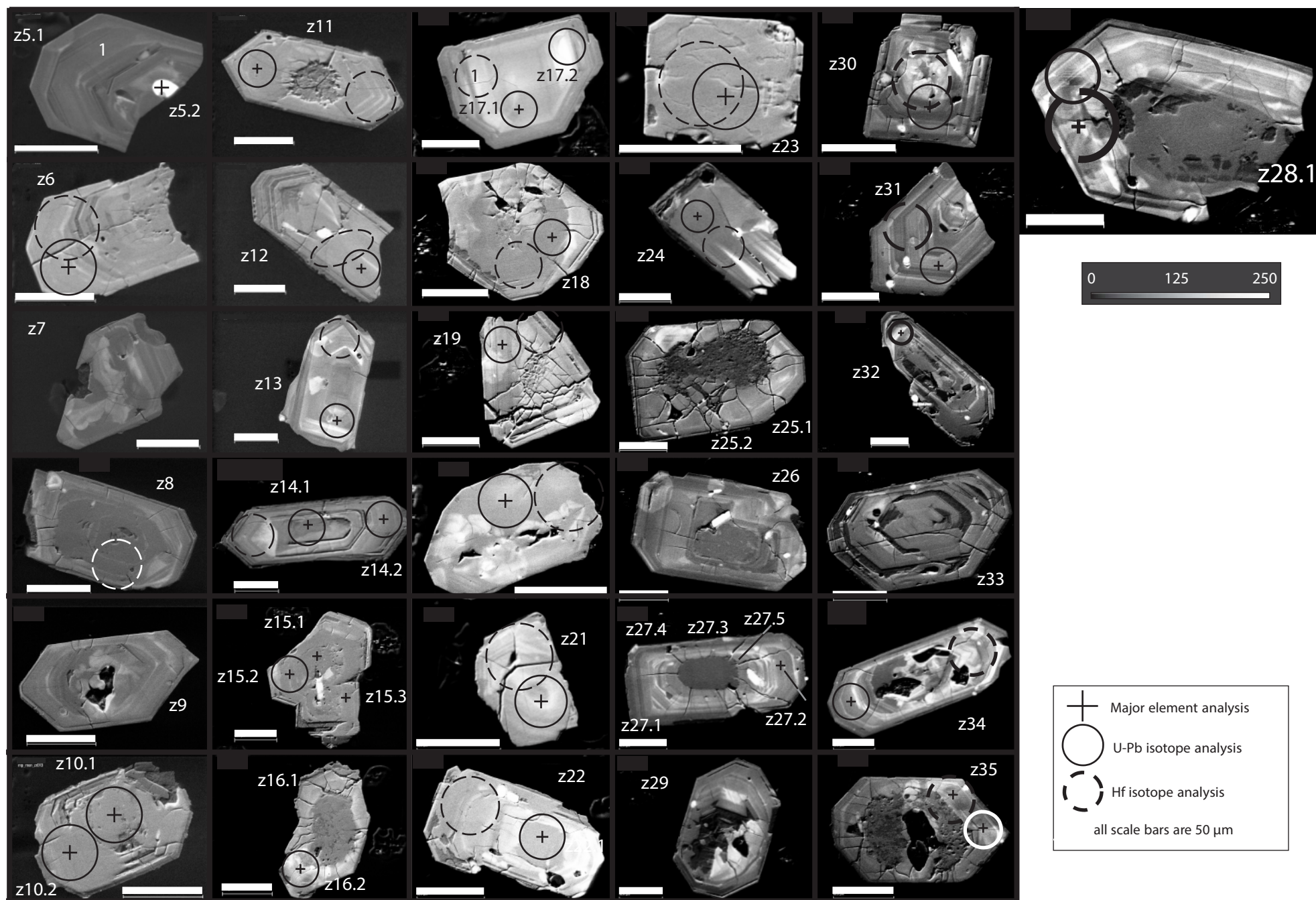
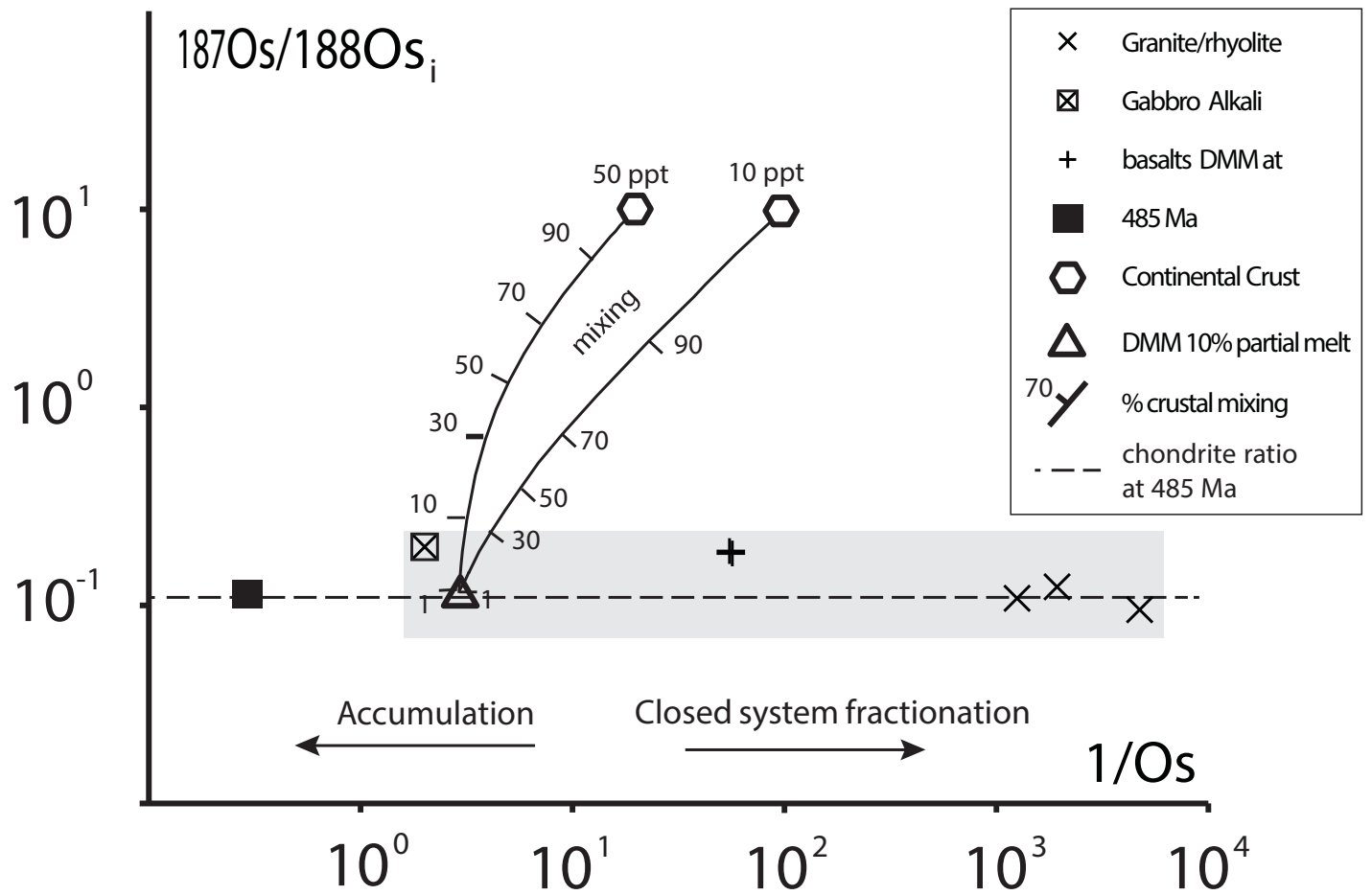


Figure 2b





a)



b)

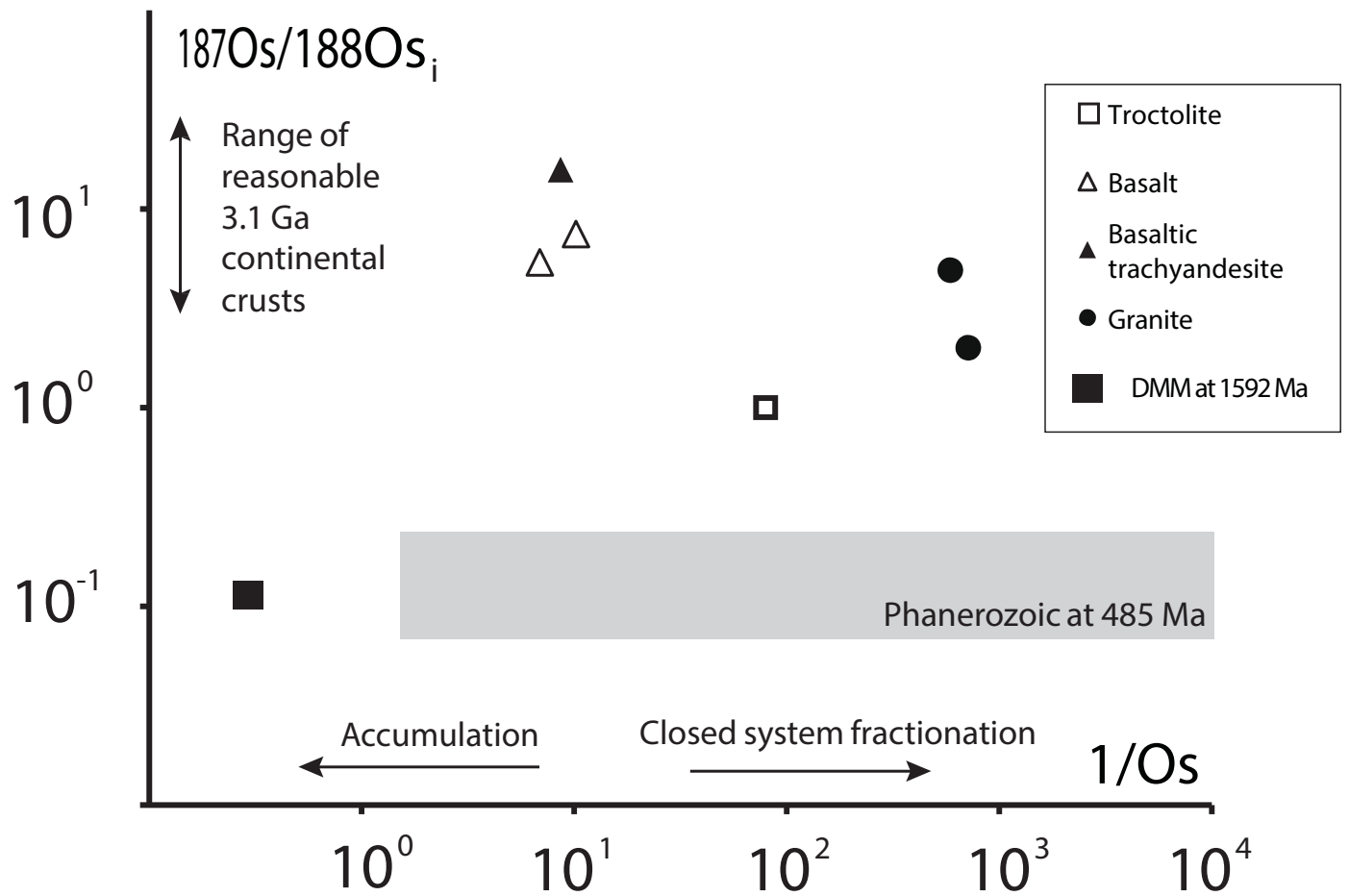


**Table 1**

In situ major, trace and isotopic data from the Marcollat Granite zircon population.

Analysis	z01	z02.1	z03.1	z03.2	z04	z05.1	z05.2	z05.3	z06.1	z06.2	z06.3	z07.1	z08	z09	z10
ZrO <sub>2</sub> (wt.%)	66.51	67.38	67.26	67.57	66.64	67.70	67.35	62.21	66.62	66.88	66.91	67.20	67.62	66.99	67.77
SiO <sub>2</sub>	32.50	32.77	32.75	32.78	32.61	32.61	32.93	31.94	32.67	32.77	32.71	32.45	32.89	32.80	32.73
HfO <sub>2</sub>	1.03	0.96	1.07	1.16	1.08	0.90	1.09	3.75	1.45	1.08	1.01	0.91	1.04	1.06	1.47
Ti <sup>a</sup> (ppm)	5.60	3.64	2.91	2.40	3.29	16.13			4.85			5.50	5.42	4.75	9.76
Y <sup>a</sup>	910.91	2118.56	2060.21	1237.84	1260.09	2070.31			1938.44			2438.62	868.98	2153.00	1539.62
Yb <sup>a</sup>	242.91	509.49	513.40	325.21	336.33	529.10			481.53			584.79	248.30	537.77	435.51
Hf <sup>a</sup>	8710.44	8135.51	9110.68	9110.68	9157.32	9281.97			8542.54			7675.05	8812.19	9024.19	12457.65
Th <sup>a</sup>	97.28	162.95	222.74	146.06	189.22	190.86			341.08			376.10	100.60	167.08	155.30
U <sup>a</sup>	140.77	179.81	399.44	247.13	279.44	313.25			361.00			350.09	140.19	180.75	205.38
<sup>207</sup> Pb/ <sup>206</sup> Pb	0.0568	0.0579	0.0563	0.0561	0.0568	0.0598			0.0574			0.0764	0.0590	0.0579	0.0564
1σ	0.0012	0.0009	0.0008	0.0008	0.0009	0.0010			0.0009			0.0012	0.0011	0.0010	0.0010
<sup>207</sup> Pb/ <sup>235</sup> U	0.5890	0.5986	0.5966	0.5950	0.5906	0.6923			0.6233			0.8381	0.6354	0.6080	0.6103
1σ	0.0119	0.0098	0.0087	0.0093	0.0093	0.0120			0.0101			0.0132	0.0120	0.0107	0.0113
<sup>206</sup> Pb/ <sup>238</sup> U	0.0752	0.0750	0.0768	0.0770	0.0754	0.0839			0.0788			0.0795	0.0781	0.0762	0.0785
1σ	0.0009	0.0009	0.0009	0.0009	0.0009	0.0011			0.0009			0.0009	0.0010	0.0009	0.0010
<sup>208</sup> Pb/ <sup>232</sup> Th	0.0246	0.0243	0.0252	0.0249	0.0244	0.0278			0.0248			0.0292	0.0252	0.0242	0.0248
1σ	0.0007	0.0006	0.0006	0.0006	0.0006	0.0009			0.0007			0.0009	0.0006	0.0006	0.0006
<sup>176</sup> Hf/ <sup>177</sup> Hf <sub>m</sub>	0.282565	0.282638	0.282581	0.282583	0.282580	0.282615		0.282610			0.282585	0.282596	0.282556	0.282600	0.282657
1σ	0.000011	0.000012	0.000009	0.000008	0.000010	0.000012		0.000009			0.000012	0.000009	0.000006	0.000007	0.000017
<sup>176</sup> Lu/ <sup>177</sup> Hf <sub>m</sub>	0.000667	0.001682	0.001826	0.001078	0.001129	0.003582		0.001871			0.001348	0.001287	0.001164	0.001589	0.003223
<sup>176</sup> Yb/ <sup>177</sup> Hf <sub>m</sub>	0.034890	0.095212	0.108550	0.063080	0.063840	0.147714		0.105373			0.074513	0.072220	0.064868	0.087574	0.111338
<sup>206</sup> Pb/ <sup>238</sup> U age (Ma)	467	466	477	478	469	519			489			493	485	474	487
1σ	6	5	5	6	5	6			6			6	6	6	6
<sup>176</sup> Hf/ <sup>177</sup> Hf <sub>i</sub> ( <sup>480</sup> Ma)	0.282559	0.282622	0.282564	0.282573	0.282569	0.282582		0.282593	0.282572			0.282584	0.282545	0.282585	0.282627
εHf	3.39	5.64	3.58	3.89	3.77	4.20		4.59	3.87			4.28	2.91	4.33	5.81
1σ	0.39	0.42	0.32	0.29	0.33	0.42		0.33	0.42			0.30	0.22	0.26	0.60

Major elements expressed in wt% oxides were analysed by EMP with a 15 kV accelerating voltage and 20 nA beam.

EMP standards used had the following composition; Hf: Hf wire (Hf, 100%); Zr, O: zircon (O, 34.78%; Si, 15.26%; P, 0.04%; Y, 0.05%; Zr, 48.97%; Hf, 0.9%); and Y: YAG (Y, 44.93%; O, 32.34%; Al, 22.73%). Pb, Th and U isotopes were measured by quadrupole ICPMS. Each mass had a dwell time of 10 ms except <sup>238</sup>U and <sup>206</sup>Pb (15 ms) and <sup>207</sup>Pb (30 ms).

Hf, Lu and Yb isotope ratios were measured by

multicollector ICPMS. bd = below detection limit.

A <sup>176</sup>Lu decay constant of  $1.93 \times 10^{-11}$  (Blichert-Toft and Albarède, 1997) was used to calculate initial <sup>176</sup>Hf/<sup>177</sup>Hf ratios.A CHUR<sub>t=0</sub> value of 0.282772 and <sup>176</sup>Lu/<sup>177</sup>Hf ratio of 0.0332 (Blichert-Toft and Albarède, 1997) was used to calculate εHf.

Hf isotope ratios with no direct corresponding major element analysis were corrected using the data from within the same grain.

<sup>a</sup>Data from the same spots analysed, see Pankhurst (2012).

**Table 1** (continued)

Analysis	z11.1	z11.2	z12	z13	z14	z15.1	z15.2	z16.1	z17.1	z18.1	z18.2	z19	z20.1	z20.2	z20.3	z21.1
ZrO <sub>2</sub> (wt.%)	68.03	68.07	66.77	66.93	67.64	66.97	67.94	67.37	67.37	67.09		67.31	67.62			66.85
SiO <sub>2</sub>	32.92	32.82	32.67	32.65	32.60	32.62	32.84	32.62	32.63	32.73		32.49	32.69			32.71
HfO <sub>2</sub>	1.03	0.90	1.43	0.89	1.51	0.99	1.47	1.15	1.20	1.06		1.86	1.16			1.25
Ti <sup>ii</sup> (ppm)	5.95	5.37	4.92	4.80	6.25	8.26	6.91	2.90	6.66	2.49		10.34	6.99			5.47
Y <sup>iii</sup>	1538.43	962.64	1007.52	1068.86	1694.32	1197.27	1296.31	1613.67	1024.57	2602.57		2510.65	2149.02			1230.94
Yb <sup>iii</sup>	350.39	254.80	289.30	281.35	462.13	320.04	359.63	421.65	280.87	634.21		675.08	544.76			337.61
Hf <sup>iii</sup>	7591.95	8698.57	12141.36	7505.46	12844.33	8400.92	12447.48	9742.43	10213.05	8957.20		15788.51	9818.74			10570.90
Th <sup>iii</sup>	152.69	112.91	91.44	127.56	251.08	143.59	94.15	151.66	108.23	208.56		337.33	267.45			127.36
U <sup>iii</sup>	160.20	155.54	168.24	164.11	367.44	172.47	127.40	253.17	156.85	261.61		528.16	416.39			175.46
<sup>207</sup> Pb/ <sup>206</sup> Pb	0.0595	0.0576	0.0580	0.0573	0.0568	0.0553	0.0555	0.0572	0.0576	0.0570		0.0568	0.1176			0.0578
1σ	0.0011	0.0010	0.0011	0.0010	0.0009	0.0011	0.0012	0.0010	0.0011	0.0009		0.0009	0.0016			0.0011
<sup>207</sup> Pb/ <sup>235</sup> U	0.6343	0.6119	0.6248	0.6198	0.6098	0.5871	0.6051	0.6198	0.6136	0.6240		0.6014	1.6011			0.5886
1σ	0.0112	0.0110	0.0122	0.0111	0.0098	0.0112	0.0134	0.0109	0.0121	0.0102		0.0096	0.0228			0.0107
<sup>206</sup> Pb/ <sup>238</sup> U	0.0774	0.0771	0.0781	0.0784	0.0779	0.0771	0.0790	0.0786	0.0773	0.0794		0.0767	0.0988			0.0739
1σ	0.0009	0.0009	0.0010	0.0010	0.0009	0.0010	0.0010	0.0010	0.0010	0.0009		0.0009	0.0012			0.0009
<sup>208</sup> Pb/ <sup>232</sup> Th	0.0249	0.0241	0.0255	0.0242	0.0240	0.0241	0.0254	0.0240	0.0246	0.0250		0.0241	0.0875			0.0229
1σ	0.0006	0.0006	0.0007	0.0007	0.0007	0.0007	0.0008	0.0008	0.0008	0.0006		0.0006	0.0023			0.0007
<sup>176</sup> Hf/ <sup>177</sup> Hf <sub>m</sub>	0.282572		0.282544	0.282578	0.282679	0.282665		0.282556	0.282555	0.282706	0.282776	0.282587	0.282723	0.282638	0.282576	0.282599
1σ	0.000008		0.000010	0.000012	0.000009	0.000012		0.000010	0.000011	0.000014	0.000014	0.000009	0.000015	0.000008	0.000009	0.000009
<sup>176</sup> Lu/ <sup>177</sup> Hf <sub>m</sub>	0.001161		0.000608	0.000865	0.001571	0.001677		0.001008	0.000748	0.002064	0.002008	0.000852	0.001345	0.000991	0.001010	0.000781
<sup>176</sup> Yb/ <sup>177</sup> Hf <sub>m</sub>	0.063857		0.033852	0.047294	0.093548	0.095373		0.059210	0.041535	0.119998	0.123863	0.052390	0.084752	0.061841	0.060226	0.046954
<sup>206</sup> Pb/ <sup>238</sup> U age (Ma)	480	479	485	487	484	479	490	488	480	493		477	607			460
1σ	6	6	6	6	6	6	6	6	6	6		5	7			5
<sup>176</sup> Hf/ <sup>177</sup> Hf <sub>i</sub> (480 Ma)	0.282561		0.282538	0.282570	0.282664	0.282649		0.282547	0.282548	0.282687	0.282757	0.282579	0.282710	0.282629	0.282567	0.282592
εHf	3.48		2.67	3.79	7.13	6.60		2.96	3.01	7.92	10.42	4.11	8.76	5.87	3.67	4.56
1σ	0.28		0.35	0.42	0.30	0.42		0.35	0.39	0.49	0.49	0.31	0.53	0.29	0.33	0.31

**Table 1** (continued)

Analysis	z22	z23	z24.1	z25	z26	z27.1	z27.2	z27.3	z28	z29	z30	z31	z32	z33
ZrO <sub>2</sub> (wt.%)	67.33	67.28	67.94	67.11	67.16	67.09	67.07	66.74	67.87	67.34	66.40	67.22	66.61	67.11
SiO <sub>2</sub>	32.74	32.61	32.77	32.74	32.84	32.86	32.77	32.61	32.31	32.64	32.57	32.71	32.64	32.73
HfO <sub>2</sub>	1.02	1.06	0.91	1.03	1.05	1.23	1.11	1.48	1.23	1.12	1.14	1.07	1.25	1.08
Ti <sup>n</sup> (ppm)	7.15	3.77	5.12	5.06	21413.19	4.90	4.01		2.45	9.14	2.84	1.87	20.19	26.94
Y <sup>n</sup>	1207.98	1264.00	909.79	1952.85	1048.84	1036.24	1555.97		1103.91	4683.60	2776.13	468.44	4727.19	1594.32
Yb <sup>n</sup>	327.51	333.88	236.28	485.68	298.13	297.54	444.05		317.80	1096.71	691.73	142.79	1125.63	434.97
Hf <sup>n</sup>	8621.40	9014.86	7746.28	8722.31	8885.97	10430.14	12565.35		10390.28	9503.30	9634.74	9077.61	10564.97	9191.24
Th <sup>n</sup>	145.26	163.74	103.38	158.81	86.03	133.08	190.52		130.90	589.28	363.28	55.56	799.19	161.86
U <sup>n</sup>	170.25	243.02	128.75	178.36	146.39	172.81	358.72		285.68	408.29	576.50	130.50	1276.19	193.76
<sup>207</sup> Pb/ <sup>206</sup> Pb	0.0582	0.0573	0.0583	0.0566	0.0592	0.0567	0.0560		0.0564	0.0556	0.0563	0.0574	0.0564	0.0588
1σ	0.0011	0.0010	0.0012	0.0011	0.0012	0.0011	0.0009		0.0010	0.0009	0.0009	0.0010	0.0010	0.0011
<sup>207</sup> Pb/ <sup>235</sup> U	0.6120	0.6145	0.6086	0.5909	0.6414	0.6228	0.5876		0.6030	0.6011	0.6085	0.5944	0.6242	0.6507
1σ	0.0115	0.0107	0.0124	0.0117	0.0132	0.0120	0.0096		0.0102	0.0103	0.0095	0.0107	0.0110	0.0117
<sup>206</sup> Pb/ <sup>238</sup> U	0.0763	0.0778	0.0757	0.0757	0.0786	0.0797	0.0761		0.0776	0.0785	0.0784	0.0751	0.0803	0.0802
1σ	0.0009	0.0009	0.0010	0.0009	0.0010	0.0010	0.0009		0.0009	0.0009	0.0009	0.0009	0.0010	0.0010
<sup>208</sup> Pb/ <sup>232</sup> Th	0.0236	0.0243	0.0240	0.0238	0.0254	0.0260	0.0240		0.0252	0.0253	0.0251	0.0237	0.0257	0.0251
1σ	0.0007	0.0008	0.0008	0.0008	0.0009	0.0007	0.0007		0.0008	0.0007	0.0008	0.0008	0.0010	0.0009
<sup>176</sup> Hf/ <sup>177</sup> Hf <sub>m</sub>	0.282636	0.282565	0.282555	0.282663	0.282566			0.282554	0.282563	0.282571	0.282552	0.282603	0.282643	0.282545
1σ	0.000010	0.000010	0.000008	0.000011	0.000010			0.000008	0.000007	0.000010	0.000009	0.000009	0.000008	0.000026
<sup>176</sup> Lu/ <sup>177</sup> Hf <sub>m</sub>	0.001964	0.000779	0.001083	0.001643	0.001976			0.000950	0.000910	0.001384	0.001644	0.001400	0.003067	0.002063
<sup>176</sup> Yb/ <sup>177</sup> Hf <sub>m</sub>	0.114020	0.043178	0.059067	0.091227	0.110493			0.048968	0.047125	0.072097	0.090061	0.079231	0.184937	0.101426
<sup>206</sup> Pb/ <sup>238</sup> U age (Ma)	474	483	471	470	488	492	469		479	478	483	474	493	509
1σ	6	6	6	6	6	8	6		6	7	6	7	7	7
<sup>176</sup> Hf/ <sup>177</sup> Hf <sub>i</sub> ( <sup>480</sup> Ma)	0.282618	0.282558	0.282545	0.282648	0.282548			0.282545	0.282555	0.282558	0.282537	0.282590	0.282614	0.282526
εHf	5.48	3.35	2.90	6.54	3.00			2.91	3.24	3.37	2.61	4.49	5.36	2.22
1σ	0.34	0.34	0.27	0.39	0.34			0.28	0.25	0.35	0.32	0.33	0.29	0.91

**Table 2**

In situ major, trace and isotopic data from the Mt Monster Porphyry zircon population.

Analysis	monzr5.1	monzr6.1	monzr7.1	monzr8.1	monzr9.1	monzr10.1	monzr10.2	monzr11.1	monzr12.1	monzr13.1	monzr14.1	monzr14.2	monzr15.1	monzr15.2	monzr16.1
ZrO <sub>2</sub> (wt.%)	63.14	64.85	65.22	63.42	64.57	59.55	63.72	64.49	64.28	64.73	63.92	64.41	63.06	63.98	61.17
SiO <sub>2</sub>	31.09	31.87	32.03	31.82	31.96	30.52	31.66	31.70	31.86	31.59	31.31	31.19	31.63	31.82	31.03
HfO <sub>2</sub>	1.42	1.52	1.25	1.84	1.66	1.40	1.65	1.46	1.08	1.10	1.20	1.47	1.78	1.73	1.83
Y <sub>2</sub> O <sub>3</sub>	0.70	0.31	0.19	0.62	0.15	2.67	0.52	0.21	0.30	0.30	0.55	0.18	0.69	0.40	1.47
P (ppm)	391.66	488.11	575.37	494.17	450.2	1146.22	408.61	834.89	457.49	789.96	421.11	428.93		681.57	
Ti	30.32	12.12	17.33	50.79	14.31	22.11	36.11	42.97	363.28	9.73	34.05	10.64		110.33	
Y	2818.55	2087.36	691.33	6210.86	2052.16	5067.97	3801.04	2279.63	5674.21	2989.23	13433.08	6941.82		7547.79	
Nb	23.91	15.97	9.6	43.25	12.42	26.45	52.42	21.14	15.13	11.86	39.23	23.95		134.62	
La	9.85	8.55	6.38	27.2	46.26	21.47	7.19	164.61	50.16	167.53	166.26	34.23		19.86	
Ce	117.68	68.94	47.54	388.17	277.4	111.37	105.94	380.87	483.41	243.05	1605.89	698.82		348.75	
Pr	6.75	3.47	2.6	17.8	13.05	9.44	4.06	32.39	14.3	31.06	59.77	29.54		9.33	
Nd	35.38	15	11.56	91.19	49.98	50.7	23.07	125.97	68.12	125.06	258.55	140.2		43.39	
Sm	19.68	9.71	7.14	54.13	22.63	27.11	16.57	27.19	42.97	34.06	138.42	81.97		27.99	
Eu	1.06	0.48	0.317	2.59	1.14	0.8	0.68	1.08	2.74	2.63	10.04	4.59		1.08	
Gd	55.19	38.54	14.57	135.56	41.82	80.32	63.76	49.92	145.4	76.63	312.36	157.95		115.86	
Tb	22.03	14.47	5.2	47.9	16.32	33.08	24.18	17.93	51.29	23.72	110.33	58.5		41.97	
Dy	265.47	179.15	61.41	555.36	179.51	432.28	318.35	196.93	579.18	266.55	1165.2	622.9		561.93	
Ho	91.88	69.54	21.72	193.07	64.91	169.43	122.98	71.37	199.35	98.98	369.77	211.12		220.56	
Er	413.73	320.46	101.73	803.24	295.77	785.09	583.6	323.64	842.5	418.73	1474.94	869.77		1044.83	
Tm	89.95	69.94	22.95	165.88	66	170.17	133.66	69.07	170.05	81.18	288.83	175.11		224.36	
Yb	858.4	670.09	219.12	1501.31	684.77	1723.93	1322.48	644.83	1521.56	730.56	2417.95	1561.59		2070.54	
Lu	143.74	116.85	41.23	234.72	115.1	299.38	223.23	114.61	257.05	128.52	346.79	239.33		352.25	
Hf	12042.99	12912.17	10592.95	15627.4	14114.6	11900.53	13951.79	12398.3	9126.79	9348.96	10158.78	12455.96		14653.92	
Ta	4.5	4.14	2.21	11.45	9.19	7.35	16.58	4.55	2	2.27	8.62	8.84		37.08	
Pb	28.8	30.18	11.48	53.3	19.04	107.69	72.35	47.43	89.37	24.83	67.73	44.22		168.61	
Th	509.34	637.99	107.64	1044.21	406.5	2016.36	1347.41	713.55	876.38	452.6	1124.7	664.48		3451.88	
U	917.12	1066.84	269.27	2146.79	1123.71	3064.94	2843.25	1075.79	851.39	679.41	1113.98	1293.27		5834.43	
<sup>207</sup> Pb/ <sup>206</sup> Pb	0.0461	0.0636	0.0461	0.0461	0.0504	0.0697	0.0713	0.0477	0.0461	0.0620	0.1389	0.0625		0.0727	0.1915
1σ	0.0066	0.0038	0.0087	0.0048	0.0035	0.0046	0.0049	0.0145	0.0209	0.0039	0.0120	0.0042		0.0056	0.0097
<sup>207</sup> Pb/ <sup>235</sup> U	0.4581	0.7058	0.4272	0.4304	0.5381	0.8775	0.8142	0.4713	0.4603	0.6361	1.0852	0.6906		0.9033	1.6561
1σ	0.0645	0.0401	0.0798	0.0440	0.0361	0.0549	0.0532	0.1421	0.2081	0.0386	0.0878	0.0447		0.0677	0.0790
<sup>206</sup> Pb/ <sup>238</sup> U	0.0722	0.0806	0.0673	0.0678	0.0775	0.0914	0.0828	0.0716	0.0725	0.0744	0.0567	0.0802		0.0902	0.0628
1σ	0.0015	0.0020	0.0020	0.0017	0.0021	0.0023	0.0023	0.0020	0.0029	0.0018	0.0019	0.0021		0.0027	0.0014
<sup>208</sup> Pb/ <sup>232</sup> Th	0.0231	0.0380	0.0233	0.0262	0.0284	0.0347	0.0349	0.0227	0.0273	0.0262	0.0163	0.0284		0.0313	0.0244
1σ	0.0021	0.0059	0.0045	0.0044	0.0051	0.0061	0.0066	0.0032	0.0061	0.0038	0.0035	0.0045		0.0058	0.0034
<sup>176</sup> Hf/ <sup>177</sup> Hf <sub>m</sub>	0.282753	0.282960	0.282805	0.282986	0.282525		0.282610	0.282673	0.282622	0.282606		0.282584		0.282584	
1σ	0.000011	0.000024	0.000012	0.000018	0.000033		0.000012	0.000040	0.000017	0.000018		0.000018		0.000013	
<sup>176</sup> Lu/ <sup>177</sup> Hf <sub>m</sub>	0.002193	0.004653	0.001665	0.003142	0.006677		0.002794	0.005446	0.002150	0.001002		0.003413		0.003413	
<sup>176</sup> Yb/ <sup>177</sup> Hf <sub>m</sub>	0.074749	0.167258	0.057288	0.137790	0.231365		0.096793	0.252503	0.075609	0.039372		0.150460		0.150460	
<sup>206</sup> Pb/ <sup>238</sup> U age (Ma)	449	499	420	423	481	564	513	446	451	462	356	497	557	393	
1σ	9	12	12	10	13	14	13	12	17	11	12	12	16	8	
<sup>176</sup> Hf/ <sup>177</sup> Hf <sub>i(485 Ma)</sub>	0.282732	0.282916	0.282789	0.282956	0.282462		0.282584	0.282622	0.282602	0.282597		0.282552		0.282552	
εHf	9.65	16.16	11.67	17.58	0.09		4.39	5.74	5.03	4.84		3.26		3.26	
1σ	0.39	0.84	0.42	0.63	1.16		0.42	1.40	0.60	0.63		0.46		0.46	

Pb isotope ratios are common Pb corrected.

Major elements expressed in wt.% oxides were analysed by EMP with a 15 kV accelerating voltage and 20 nA beam.

EMP standards used had the following composition; Hf: Hf wire (Hf, 100%); Zr, O: zircon (O, 34.78%; Si, 15.26%; P, 0.04%; Y, 0.05%; Zr, 48.97%; Hf, 0.9%); and Y: YAG (Y, 44.93%; O, 32.34%; Al, 22.73%).

Concentrations calculated by quadrupole ICPMS on measured isotopes as follows; <sup>31</sup>P, <sup>49</sup>Ti, <sup>89</sup>Y, <sup>93</sup>Nb, <sup>139</sup>La, <sup>140</sup>Ce, <sup>141</sup>Pr, <sup>146</sup>Nd, <sup>147</sup>Sm, <sup>151</sup>Eu, <sup>157</sup>Gd, <sup>159</sup>Tb, <sup>163</sup>Dy, <sup>165</sup>Ho, <sup>166</sup>Er, <sup>169</sup>Tm, <sup>173</sup>Yb, <sup>175</sup>Lu, <sup>178</sup>Hf, <sup>181</sup>Ta, <sup>208</sup>Pb, <sup>232</sup>Th and <sup>238</sup>U. Each mass had a dwell time of 10 ms except <sup>238</sup>U and <sup>206</sup>Pb (15 ms) and <sup>207</sup>Pb (30 ms).

Hf, Lu and Yb isotope ratios were measured by multicollector ICPMS.

A <sup>176</sup>Lu decay constant of  $1.93 \times 10^{-11}$  (Blichert-Toft and Albarède, 1997) was used to calculate initial <sup>176</sup>Hf/<sup>177</sup>Hf ratios.

A CHUR<sub>t = 0</sub> value of 0.282772 and <sup>176</sup>Lu/<sup>177</sup>Hf ratio of 0.0332 (Blichert-Toft and Albarède, 1997) was used to calculate εHf.

**Table 2 (continued)**

Analysis	monzr16.2	monzr17.1	monzr17.2	monzr18.1	monzr19.1	monzr20.1	monzr21.1	monzr22.1	monzr23.1	monzr24.1	monzr25.1	monzr25.2	monzr26.1	monzr27.1	monzr27.1	monzr27.1
ZrO <sub>2</sub> (wt.%)	62.53	64.82	64.77	62.93	64.01	63.14	63.96	62.59	62.40	63.11	62.00	64.85	61.16	63.16	60.66	60.34
SiO <sub>2</sub>	31.12	30.52	32.09	30.99	30.93	31.39	31.26	30.75	30.94	30.46	31.96	30.90	30.15	30.60	29.86	29.94
HfO <sub>2</sub>	1.53	1.20	1.52	1.74	1.71	3.12	1.61	1.12	1.58	1.10	1.72	1.40	1.01	1.87	1.81	1.76
Y <sub>2</sub> O <sub>3</sub>	0.27	0.34	0.25	0.91	0.40	0.19	0.41	1.44	0.96	1.16	0.99	0.20	2.07	0.77	1.94	1.85
P (ppm)	7198.93	438.99	353.7	573.81	361.88	202.11	346.27	553.41	1314.43	574.62	232.58		786.91	1670.52		412.46
Ti	287.15	11.99	14.1	76.85	231.35	28.44	35.58	16.62	238.74	54.29	267.42		25.59	15.09		6.24
Y	12919.22	3080.3	1680.24	4189.85	5503.85	2563.22	2063.13	4146.13	9941.12	5919.92	1687.95		9567.09	13663.27		2272.54
Nb	56.08	6.9	5.24	53.78	80.63	66	31.67	36.23	85.68	23.44	26.29		66.16	86.51		14.97
La	72.77	0.802	0.774	15.14	18.54	9.54	3.01	20.37	61.96	4.94	3.42		18.08	1.7		3.33
Ce	1842.44	37	19.55	87.28	371.18	106	47.26	290.88	448.62	87.67	98.14		295.42	74.93		74.56
Pr	39.83	0.746	0.367	4.6	13.12	5.43	1.88	14.23	22.38	3.33	1.76		9.31	1.4		1.45
Nd	214.98	7.4	3.84	23.05	67.37	21.48	8.94	68.46	99.81	23.46	11.44		57.36	12.15		9.27
Sm	133.66	13.36	6.43	14.31	49.99	12.82	7.57	38.39	63.93	32.67	8.44		64.69	29.04		9.59
Eu	8.67	1.5	0.649	0.426	2.54	1	0.48	1.46	2.63	3.99	0.72		3.09	0.5		0.499
Gd	307.04	66.11	32.66	61.37	126.39	32.47	32.59	88.25	192.19	153.9	30.87		244.76	176.71		38.71
Tb	109.34	25.69	12.14	24.7	42.31	13.31	11.51	32.56	71.38	51.92	13.41		90.36	79.01		14.77
Dy	1188.82	289.69	153	325.78	489.42	168	158.68	376.17	843.87	586.89	148.12		1012.91	1069.96		182.8
Ho	380.94	108.7	58.92	136.19	174.19	62.39	66.66	132	314.27	209.9	57.55		356.13	450.14		72.73
Er	1530.84	466.58	260.98	660.19	755.17	299.74	331.4	600.75	1446.79	880.3	253.01		1447.31	2174.86		349.58
Tm	310.29	94.07	53.6	150.71	160.67	81.36	78.57	125.66	303.73	170.19	58.75		276.81	495.86		77.2
Yb	2962.93	868.8	497.88	1460.3	1545.97	955.31	788.47	1148.63	2811.93	1505.29	584.59		2451.35	4895.93		751.85
Lu	423.16	153.89	91.99	262.94	254.62	185.22	139.32	201.41	490.92	261.5	96.65		389.29	845.65		134.83
Hf	15519.71	10163.87	10163.87	14748.05	14512.31	26462.87	13655.85	9508.38	13437.92	9300.63	14608.98		8575.6	15836.84		13536.28
Ta	11.91	1.99	1.538	18.77	13.4	218	9.28	5.07	16.94	3.51	5.58		10.91	28.6		5.11
Pb	91.81	28.4	20.65	118.37	57.44	11.4	26.87	47.8	192.88	57.29	16.55		200.05	270.56		36.65
Th	1917.67	557.32	376.87	2139.3	1066.62	138.09	674.94	885.55	3821.98	1131.7	353.21		4042.98	6476.62		714.01
U	1648.38	627.9	475.25	4173.12	2262.44	2656.37	1521.76	1232.45	5349.61	1002.46	747.42		2763.75	13851.59		1251.86
<sup>207</sup> Pb/ <sup>206</sup> Pb		0.0671	0.0618	0.0605	0.0461	0.0608	0.0556	0.0536	0.0728	0.0595	0.0717		0.0711	0.0560		0.0583
1σ		0.0024	0.0035	0.0026	0.0192	0.0033	0.0035	0.0116	0.0045	0.0040	0.0066		0.0051	0.0040		0.0041
<sup>207</sup> Pb/ <sup>235</sup> U		0.7359	0.6791	0.6657	0.4264	0.6640	0.6082	0.5674	0.7856	0.6134	0.7640		0.8116	0.6182		0.6821
1σ		0.0249	0.0369	0.0270	0.1763	0.0350	0.0371	0.1217	0.0466	0.0386	0.0662		0.0548	0.0414		0.0457
<sup>206</sup> Pb/ <sup>238</sup> U		0.0795	0.0797	0.0799	0.0672	0.0793	0.0794	0.0768	0.0783	0.0747	0.0776		0.0827	0.0801		0.0849
1σ		0.0013	0.0018	0.0014	0.0031	0.0019	0.0021	0.0018	0.0019	0.0020	0.0028		0.0022	0.0021		0.0022
<sup>208</sup> Pb/ <sup>232</sup> Th		0.0258	0.0269	0.0268	0.0458	0.0499	0.0263	0.0240	0.0231	0.0262	0.0329		0.0354	0.0316		0.0361
1σ		0.0020	0.0033	0.0031	0.0222	0.0080	0.0049	0.0016	0.0041	0.0051	0.0088		0.0070	0.0070		0.0074
<sup>176</sup> Hf/ <sup>177</sup> Hf <sub>m</sub>		0.282651		0.282606		0.282631	0.282662	0.282623	0.282640	0.282643	0.282554		0.282621			
1σ		0.000015		0.000017		0.000025	0.000018	0.000014	0.000027	0.000018	0.000017		0.000023			
<sup>176</sup> Lu/ <sup>177</sup> Hf <sub>m</sub>		0.001850		0.002267		0.002896	0.002685	0.001984	0.004544	0.001991	0.002299		0.002943			
<sup>176</sup> Yb/ <sup>177</sup> Hf <sub>m</sub>		0.065366		0.094357		0.088906	0.102672	0.082077	0.149879	0.078271	0.081486		0.100981			
<sup>206</sup> Pb/ <sup>238</sup> U age (Ma)		493	495	495	419	492	492	477	486	465	482		512	496		525
1σ		8	11	8	19	11	12	11	11	12	17		13	13		13
<sup>176</sup> Hf/ <sup>177</sup> Hf <sub>i</sub> (485 Ma)		0.282634		0.282585		0.282604	0.282637	0.282604	0.282597	0.282624	0.282532		0.282593			
εHf		6.15		4.42		5.10	6.27	5.12	4.87	5.82	2.57		4.73			
1σ		0.53		0.60		0.88	0.63	0.49	0.95	0.63	0.60		0.81			

**Table 2 (continued)**

Analysis	monzr27.4	monzr27.5	monzr28.1	monzr28.2	monzr29.1	monzr30.1	monzr31.1	monzr31.2	monzr32.1	monzr33.1	monzr34.1	monzr35			
ZrO <sub>2</sub> (wt.%)	63.49	64.67	64.03	62.76	63.94	64.01	62.76		64.28	63.67	64.63	63.24			
SiO <sub>2</sub>	30.88	30.87	30.87	31.10	30.16	30.86	30.36		30.67	31.55	31.79	30.27			
HfO <sub>2</sub>	1.60	1.39	1.35	1.82	1.42	1.47	1.44		1.58	1.01	1.45	1.23			
Y <sub>2</sub> O <sub>3</sub>	0.51	0.25	0.44	0.62	0.42	0.39	0.46		0.29	1.05	0.23	1.25			
P (ppm)			192.16	590.7	288.87	773.26	598.49		388.35	446.32	310.96	565.21	47.49	52.18	47.57
Ti			33.87	46.86	84.1	68.65	37.18		270.87	1113.21	9.53	124.01	12.43	23.93	11.47
Y			581.5	2097.13	2991.78	4227.69	3253.09		6381.11	9036.57	1897.11	4294	3.68	3.73	3.67
Nb			3.89	23.08	16.02	44.94	29.94		40.13	39.75	9.19	87.07	4.44	5.66	4.19
La			1	9.88	45.24	12.42	6.3		53.08	163.96	1.8	33.74	5.79	10.59	4.98
Ce			18.51	133.21	364.98	137.72	99.32		1375.29	1510.76	51.84	444.29	3.84	4.21	3.84
Pr			0.567	5.18	15.02	5.46	3.43		41.96	50.53	1.375	16.8	5.90	11.99	4.99
Nd			2.69	29.07	57.23	29.39	23.14		183.72	192.74	7.45	80.8	5.99	10.78	5.27
Sm			2.23	16.42	48.07	20.77	20.33		86.61	91.09	7.07	49.5	6.84	12.91	6.27
Eu			0.414	0.72	1.64	1.07	0.74		4.49	5.91	0.391	2.66	14.30	27.08	14.00
Gd			8.87	46.16	62.47	74.23	66.42		153.17	224.18	30.03	108.04	4.84	7.13	4.55
Tb			3.74	15.41	27.16	27.98	21.7		60.08	80.83	12.29	39.08	4.00	5.19	3.89
Dy			44.52	177.54	286.99	352.46	272.7		663.54	912.53	152.18	385.31	3.72	4.48	3.71
Ho			17.65	65.57	97.94	135.66	105.61		206.79	302.39	59.71	123.01	3.52	3.96	3.51
Er			90.03	295.72	425.73	640.35	487.86		868.99	1163.7	279.52	497.07	3.34	3.60	3.30
Tm			21.54	63.92	90.82	142.64	101.14		186.66	231.31	61.01	100.4	3.45	3.78	3.42
Yb			233.21	603.22	843.94	1368.77	948.61		1678.71	2012.58	593.75	914.42	3.69	4.25	3.71
Lu			50.47	108.85	125.17	238.1	179.15		252.17	295.85	104.05	141.51	3.32	3.52	3.30
Hf			11471.45	11471.45	12071.82	12483.09	12204.11		13393.82	8534.05	12333.85	8479.79	3.17	3.18	3.17
Ta			0.869	4.28	2.52	11.37	7.13		5.68	8.6	3.29	10.07	4.97	8.33	4.66
Pb			33.11	25.24	45.14	85.5	48.91		50.4	71.86	22.49	51.74	4.29	6.23	4.09
Th			112.28	467.61	324.28	1686.28	912.24		483.19	930.24	491.98	1744.5	3.55	3.80	3.54
U			423.54	937.36	466.05	2782.79	1410.6		1176.73	1161.05	851.3	1353.94	3.30	3.49	3.33
<sup>207</sup> Pb/ <sup>206</sup> Pb			0.2273	0.04605	0.0461	0.0614	0.0590		0.0461	0.0461	0.0550	0.1062			
1σ			0.0134	0.011	0.0071	0.0046	0.0062		0.0294	0.0296	0.0042	0.0094			
<sup>207</sup> Pb/ <sup>235</sup> U			18.7428	0.47015	0.4258	0.6587	0.6328		0.3293	0.3820	0.5861	1.1481			
1σ			1.0530	0.11157	0.0648	0.0474	0.0632		0.2092	0.2443	0.0423	0.0947			
<sup>206</sup> Pb/ <sup>238</sup> U			0.6010	0.07405	0.0671	0.0781	0.0782		0.0519	0.0602	0.0774	0.0785			
1σ			0.0145	0.00209	0.0019	0.0022	0.0030		0.0032	0.0034	0.0021	0.0026			
<sup>208</sup> Pb/ <sup>232</sup> Th			0.1469	0.02382	0.0286	0.0293	0.0297		0.0250	0.0320	0.0265	0.0321			
1σ			0.0267	0.00395	0.0063	0.0069	0.0100		0.0139	0.0133	0.0056	0.0086			
<sup>176</sup> Hf/ <sup>177</sup> Hf <sub>m</sub>				0.282595	0.282629	0.282604	0.282649	0.282589	0.282655	0.282545	0.282622	0.282600			
1σ				0.000018	0.000031	0.000015	0.000017	0.000019	0.000033	0.000073	0.000012	0.000015			
<sup>176</sup> Lu/ <sup>177</sup> Hf <sub>m</sub>				0.003105	0.001493	0.003866	0.001703	0.003245	0.002687	0.003616	0.001746	0.001761			
<sup>176</sup> Yb/ <sup>177</sup> Hf <sub>m</sub>				0.098094	0.060729	0.150997	0.068288	0.103692	0.126253	0.151482	0.063832	0.052047			
<sup>206</sup> Pb/ <sup>238</sup> U age (Ma)			3034	461	418	485	486		326	377	481	487			
1σ			58	13	11	13	18		20	21	13	16			
<sup>176</sup> Hf/ <sup>177</sup> Hf <sub>i</sub> (485 Ma)				0.282566	0.282615	0.282568	0.282633	0.282558	0.282630	0.282511	0.282606	0.282583			
εHf				3.75	5.49	3.82	6.13	3.49	6.02	1.81	5.16	4.38			
1σ				0.63	1.09	0.53	0.60	0.67	1.16	2.56	0.42	0.53			

**Table 3**

**Re–Os and Lu–Hf isotope data from Delamerian and Gawler FLIP (and related) A-type systems.**

Seismograph Granite Lu/Hf isotope ratios calculated from values in Turner et al. (1992), using Yb/Lu = 4.24 and Zr/Hf = 16.7. GRV Hf and Os data from Fricke (2005). White Hill Hf data from Frost (2009). MGO3009 from Gregory et al. (2008), age from references therein. Seismograph Granite, Black Hill peridotite ages from Turner et al. (1992). Truro Volcanics age from Foden et al. (2002a).

Name	Cambrian–Ordovician samples						Proterozoic samples					
	Marcollat Granite	Mt Monster Porphyry	Seismograph Granite	Black Hill peridotite	Truro Volcanic	Truro Volcanic	Sybella Granite	Sybella Granite	Chitanilga	Roopena	Roopena	White Hill
Sample #	PG11-2727	2001	2000		876–1013	876–1013 (dup)	7820–5068	MGO3009	C-CH-16	697440	697443	WTH101
Age (Ma)	480 ± 2.5	485 ± 7.9	490	490	522	522	1560	1560	1592	1592	1592	1592
Os (ppb)	0.000800	0.000518	0.000211	0.405300	0.017642	0.018190	0.001700	0.001400	0.115700	0.145000	0.098000	0.011800
2σ	0.0000100	0.0000026	0.0000011	0.0020265	0.0000882	0.0000909	0.0000085	0.0000070	0.0005785	0.0007250	0.0004900	0.0000500
Re (ppb)	0.00125	0.00350	0.00101	0.17983	0.02144	0.02144	0.01044	0.01373	0.82515	0.83689	0.47645	0.02076
2σ	0.00002	0.00005	0.00002	0.00270	0.00032	0.00032	0.00016	0.00021	0.01238	0.01255	0.00715	0.00031
<sup>187</sup> Os/ <sup>188</sup> Os <sub>m</sub>	0.268857	0.82521	0.58663	0.242445	0.23431	0.23786	6.31870	3.83774	18.89474	6.74690	8.77818	1.567800
2σ	0.000670	0.01	0.01	0.000360	0	0	1.1634	0.02	0.03	0.06	0.01	0.004420
<sup>187</sup> Re/ <sup>188</sup> Os <sub>m</sub>	19.19	85.73	56.41	5.46	5.93	5.76	53.40	70.10	118.50	51.80	49.80	23.13
1σ	0.37	1.36	0.89	0.09	0.09	0.09	0.84	1.11	1.87	0.82	0.79	0.36
<sup>187</sup> Os/ <sup>188</sup> Os <sub>s</sub>	0.114813	0.129723	0.105155	0.197673	0.182511	0.187547	4.912663	2.036327	15.709744	5.354639	7.439681	0.946996
	In-situ zircon			In-situ zircon			Whole rock					
	Max	Min	Average	Max	Min	Average	Seismograph Granite	Chitanilga	Roopena	Roopena	White Hill	
Hf (ppm)							15.0	5.91	4.00	4.23	0.07	
Lu							1.5	0.53	0.49	0.50	0.03	
<sup>176</sup> Hf/ <sup>177</sup> Hf <sub>m</sub>	0.282776	0.282544	0.282603	0.282986	0.282525	0.282652	0.282701	0.282168	0.282356	0.282397	0.283533	
1σ	0.000028	0.000020		0.000036	0.000066		0.000020	0.000011	0.000011	0.000020	0.000033	
<sup>176</sup> Lu/ <sup>177</sup> Hf <sub>m</sub>	0.002008	0.000608		0.003142	0.006677		0.013925	0.015400	0.017405	0.016699	0.057683	
<sup>176</sup> Hf/ <sup>177</sup> Hf <sub>i</sub>	0.282757	0.282538	0.282590	0.282956	0.282462	0.282625	0.282569	0.281687	0.281813	0.281875	0.281733	
εHf (t)	10.42	2.67	4.50	17.58	0.09	5.74	3.97	−1.73	2.73	4.95	−0.10	
1σ	0.49	0.35		0.63	1.16		0.71	0.40	0.37	0.69	1.16	